AIAA JOURNAL
Vol. 53, No. 7, July 2015

Near-Field and Acoustic Far-Field Response of a High-Speed Jet to Excitation

M. Crawley*
The Ohio State University, Columbus, Ohio 43235
A. Sinha†
Indian Institute of Technology Bombay, Powai, Mumbai 400076, India
and
M. Samimy‡
The Ohio State University, Columbus, Ohio 43235

DOI: 10.2514/1.J053581

The near-field and acoustic far-field response of an unheated Mach 0.9 jet with Reynolds number 6.2×10^5 was investigated. The study included both the baseline and controlled jets utilizing plasma actuators. Simultaneous acquisition of the near- and far-field signals with the actuation phase enabled the use of phase averaging to reconstruct the signature of the large-scale coherent structures generated by excitation of instabilities in the shear layer of the jet. Decomposition of the near-field pressure into its constitutive hydrodynamic and acoustic fields is accomplished via the application of a filter in the frequency/wave-number domain. The results showed that both the hydrodynamic and acoustic response to excitation for Strouhal numbers St_{DF} less than 0.50 could be well predicted by a simple linear superposition of the impulse response of the jet. The results appear to indicate that the dominant acoustic radiation reaching the far-field aft angles is being generated over an extended region of the jet mixing layer: the upstream portion of the jet, just before the end of the potential core, with highly temporally intermittent bursts occurring downstream of the potential core. Significantly lower temporal coherency of the acoustic response was found when compared to the hydrodynamic response. Finally, excitation for $St_{\mathrm{DF}} > 0.15$, which produces coherent interactions between the generated large-scale structures, was found to increase the temporal coherency of the acoustic response.

Nomenclature

a_∞	=	ambient speed of sound, m/s
D	=	nozzle-exit diameter, m
f	=	spectral frequency, Hz
Re_D	=	Reynolds number based on exit diameter and nozzle-exit conditions
St_D	=	Strouhal number based on jet-exit diameter, fD/U_j
St_{DF}	=	Strouhal number for excitation, fD/U_j
U_c	=	convective velocity for large-scale structures, m/s
U_j	=	jet-exit velocity, m/s
y	=	radial coordinate normal to the jet axis, m
τ_{ac}	=	expected time of arrival for on-axis acoustic wave, s
τ_{con}	=	expected time of arrival for hydrodynamic wave, s
τ_s	=	expected time of arrival for off-axis acoustic wave, s

I. Introduction

THE acoustic radiation generated by jet engines, the dominant source of which is the high-velocity exhaust during takeoff, has long been an issue for the aviation industry. On the commercial side, escalating number of flights, encroachment of urban and residential areas near airports, and tightening of environmental regulations have combined to force airports to institute curfews, surcharges, and flight-path restrictions to combat noise pollution. For the military, hearing damage inflicted on nearby personnel on aircraft carriers has necessitated the implementation of noise-reduction concepts on tactical aircraft, usually geometric modifications to the nozzle, which have an associated penalty in engine performance. To meet the noise-reduction and performance requirements for future aircraft engines, novel flow-control strategies must be implemented. To do this effectively, a complete understanding of the aeroacoustic noise-generation mechanism is necessary, a challenge, which, as of yet, remains unfulfilled.

The field of aeroacoustic research was pioneered over six decades ago by Lighthill, who showed that the established governing equations for fluid dynamics could be rearranged into an inhomogeneous wave equation, in which a stress tensor, comprising Reynolds stress, shear stress, and density-fluctuation terms, is the source [1]. As this acoustic analogy is exact, full knowledge of the source term would yield an exact solution for the far-field acoustic radiation. However, for jets of practical interest, a full description of the source term is not currently available, either experimentally or numerically, forcing researchers to use simplified models.

Given the stochastic description of turbulent shear layers commonly held at the time, early work used random, uncorrelated eddies as a source model. While this source model, and the resulting U_j^8 power law it produced, found some success, it was shown [2] to be deficient in explaining many aspects of jet noise, in particular, the directivity of acoustic radiation in subsonic jets. Following the discovery of coherent structures in turbulent shear layers by Mollo-Christensen [3] and later Crow and Champagne [4] and Brown and Roshko [5], source models of increasing complexity based on coherent eddies have been suggested by researchers. These axially extended waveforms have been identified as having wave-packet characteristics [6], which has led to the frequency-domain description of the large-scale structures as instability waves. Spatial modulation of the wave packet was shown to produce the superdirective character of far-field acoustic radiation observed in subsonic jets [7]. (In fact, this modulation is necessary for subsonically convecting structures to radiate to the far field [6].) Similarly, temporal modulation of the wave packet, in terms of

Presented as Paper 2014-0527 at the 52nd AIAA Aerospace Sciences Meeting, National Harbor, MD, 13–17 January 2014; received 26 April 2014; revision received 25 October 2014; accepted for publication 27 October 2014; published online 5 February 2015.

*Graduate Research Assistant, Department of Mechanical and Aerospace Engineering, Gas Dynamics and Turbulence Laboratory, Aerospace Research Center. Student Member AIAA.

†Assistant Professor, Department of Aerospace Engineering. Member AIAA.

‡Nordholt Professor of Mechanical and Aerospace Engineering, Director, Gas Dynamics and Turbulence Laboratory, Aerospace Research Center; Samimy.1@osu.edu. Fellow AIAA (Corresponding Author).

amplitude and envelope, has been shown to improve agreement between analytic models and the numerical results in terms of directivity and amplitude [8,9].

Much of the difficulty in identifying the aeroacoustic-source terms revolves around the dissimilar range of scales and fluctuation intensities of the turbulent eddies in the shear layer and the radiated noise. In the irrotational near field of the jet, strong hydrodynamic pressure fluctuations associated directly with the passage of coherent structures in the shear layer coexist with the resultant weak acoustic radiation [10]. Beyond this, in the acoustic far field, the hydrodynamic signature of the coherent structures is nonexistent, owing to their strong exponential decay with radial distance. It is in the irrotational near field that much work has focused, to improve the understanding of the link between shear-layer turbulence and far-field acoustic radiation.

Owing to the presence of strong hydrodynamic fluctuations dominating the irrotational pressure field near the noise-source regions, identification of acoustic waves and their corresponding source events is problematic, requiring a decomposition of the pressure field into its constitutive hydrodynamic and acoustic components. By identification and prediction of coherence nulls in the near field, Coiffet et al. [11] showed that the full irrotational near field consists primarily as a linear superposition of its hydrodynamic and acoustic components, which led subsequent researchers to propose linear filters to extract the individual components, with varying degrees of success. Tinney and Jordan [12] used a Fourier-based wave-number/frequency filter to separate the supersonically and subsonically convecting waves (and hence, the acoustic and hydrodynamic components) in an unheated subsonic jet. Grizzi and Camussi [13] employed an iterative approach, in which the pressure field was decomposed based on an energy threshold of the wavelet coefficients computed via the discrete wavelet transform. The energy threshold was set by an analysis of two-point correlations of the acoustic and hydrodynamic components between two microphones, to ensure physically representative propagation velocities for the decomposed components. Finally, Kuo et al. [14] proposed the use of empirical mode decomposition (EMD), in which a fluctuating signal at a single point is linearly decomposed into intrinsic mode functions to separate the individual components. In the current work, the decomposition of the hydrodynamic and acoustic components is accomplished via the application of a Fourier-based wave-number/frequency filter, as in Tinney and Jordan [12].

The Gas Dynamics and Turbulence Laboratory (GDTL) has developed a class of plasma actuators, referred to as localized arc-filament plasma actuators (LAFPAs), which can provide excitation signals of high amplitude and high frequency required for the control of high-Mach-number and high-Reynolds-number jets [15,16]. The GDTL has used these actuators for noise mitigation and flow control in Mach 0.9 [17,18], Mach 1.3 [19–21], and Mach 1.65 [22] unheated jets, and has recently expanded the use of LAFPAs to heated jets [23]. A review of the development of LAFPAs and their use in flow control and fluid-phenomena research in high-speed high-Reynolds-number jets, both heated and unheated, can be found in Samimy et al. [24]. More recently, the diagnostic potential of LAFPAs for understanding the jet-flow phenomena has been explored. Excitation of instabilities in the flow by LAFPAs results in a definitive spatiotemporal origin to which resulting phenomena can be referenced. The absolute temporal reference afforded by the LAFPA excitation provides researchers the ability to investigate the growth, saturation, and decay of structures with high fidelity. Kearney-Fischer et al. [25] investigated Mach wave radiation from heated, high-Mach-number jets using schlieren imaging phase locked to LAFPAs, among other data-acquisition techniques.

Of particular importance to the current work are the results of Sinha et al. [26], which showed the quasi linearity of large-scale structure interaction through phase averaging of the near-field pressure in jets forced at low-to-moderate Strouhal numbers ($St_{DF} < 0.5$). The perturbations (instability waves) generated by the excitation grow into large-scale structures, which are observed in the irrotational near-field pressure as a compact waveform composed of a compression wave followed by an expansion. Because the compact waveform has a temporal scale far less than the excitation period at very low Strouhal numbers ($St_{DF} < 0.1$), the structures advect through the shear layer without interacting with each other, a behavior designated the impulse response of the jet by the researchers. As the excitation Strouhal number is increased, the generated structures began interacting with each other (the periodic response of the jet). It was found that, in the periodic regime, the phase-averaged response could be reproduced by a simple linear superposition of the impulse response, indicating a predominantly quasi-linear interaction of the large-scale structures in the irrotational near field. Lastly, the behavior of the seeded structures was found to be well predicted by linear parabolized stability theory.

In the present work, the methodology of Sinha et al. [26] has been extended to encompass a greater region of the near field as well as the acoustic far field. In addition, the acoustic-source region, the linearity, and the coherence of the acoustic response to excitation are evaluated by two-point space–time correlations, phase averaging, and wavelet transform, respectively.

II. Experimental Methodology

All experiments were conducted at the GDTL within the Aerospace Research Center at The Ohio State University. Compressed, dried, and filtered air is supplied to the facility from two cylindrical storage tanks with a total capacity of 43 m^3 and maximum storage pressure of 16 MPa. The air may be routed through a storage heater (not used in this study), which allows the jet to operate with a stagnation temperature up to 500°C, before expanding through a nozzle and exhausting horizontally into an anechoic chamber. Opposite the nozzle, a collector accumulates the jet and entrained air, and exhausts to the outdoors. A schematic of the anechoic chamber can be seen in Fig. 1. The dimensions of the chamber are 6.20 m wide by 5.59 m long and 3.36 m tall, with internal wedge-tip to wedge-tip dimensions of 5.14 by 4.48 and 2.53 m, respectively. The design of the chamber produces a cutoff frequency of 160 Hz, below the frequencies of interest for this study. A more detailed description of the GDTL anechoic-chamber properties and validation has been given by Hahn [27].

For this study, a converging, axisymmetric nozzle with exit diameter D of 25.4 mm (1 in.) was used. The internal contour of the nozzle was designed using a fifth-order polynomial. The nozzle used a thick-lipped design to simplify the mounts for the LAFPA extension, which housed the eight actuators used in this study. For the experiments reported in this paper, the jet was operated at a Mach number M_j of 0.90, and with a total temperature ratio of approximately unity. The Reynolds number based on the jet-exit diameter was 6.2×10^5; previous investigations using hot-wire anemometry have indicated that the initial shear layer is turbulent for this operating condition with momentum thickness ~0.09 mm and boundary-layer thickness ~1 mm [28].

A. Localized Arc-Filament Plasma Actuators

Each LAFPA consists of a pair of tungsten pin electrodes, which are placed around the nozzle perimeter 1 mm upstream of the nozzle exit. Eight uniformly spaced actuators are used in this study. The center-to-center spacing between electrode pairs for each actuator is 4 mm. The electrodes are housed in a boron nitride extension attached to the end of the nozzle. A groove with dimensions of 1 mm wide and 0.5 mm deep is machined in the boron nitride, into which the electrode tips protrude to provide a region of low-momentum flow to stabilize the plasma arcs. It has been shown that the existence of this groove does not substantially alter the flowfield or the control authority of the LAFPAs [29]. A more detailed description of the LAFPA characteristics can be found in Utkin et al. [16].

The LAFPAs are energized by a multichannel, high-voltage plasma power generator capable of simultaneously powering up to eight LAFPAs, which was designed and built in-house at the GDTL. In the second-generation power supply, each individual circuit consists of a switchable capacitor in line with a high-voltage transformer; the arcing electrodes are connected to the secondary side of the coil. The capacitor is charged by a 100 V dc power supply when the first switch is closed and the second is opened; at the user-specified time, the switches flip and it discharges through the coil.

The switches are controlled by a 16-channel digital I/O card and the National Instruments LabVIEW software, operated by a dedicated computer. The plasma generator provides independent control of the frequency, duty cycle/pulse width, and phase of each individual actuator (although at a constant amplitude of 5 kV). The pulse width was held constant at 7 μs, which was found to be the minimum pulse width at which the actuators consistently arced for all frequencies explored in this study [29]. The circuit is capable of operating at up to 100 kHz, although in the current work, it is limited to 20 kHz due to thermal concerns. To improve our understanding of the linear and nonlinear dynamics of the large-scale structure interactions, the excitation Strouhal numbers range from 0.02 to 0.50; an azimuthal mode of $m = 0$ was used in all cases.

B. Data Acquisition

Near-field and far-field pressure measurements were acquired simultaneously using Brüel & Kjær 1/4 in. 4939 microphones. The signal from each microphone is bandpass filtered from 20 Hz to 100 kHz using a Brüel & Kjær Nexus 2690 conditioning amplifier, and recorded using the National Instruments PXI-6133 A/D boards and LabVIEW software. The microphones are calibrated using a Brüel & Kjær 114 dB, 1 kHz sine wave generator. The frequency response of the microphones is flat up to roughly 80 kHz, with the protective grid covers removed. Voltage signals are collected at 200 kHz with 81,920 data points per block; subblocks of 8192 data points were used when calculating short-time power spectral densities, resulting in a frequency resolution of 24.4 Hz. Ten blocks were recorded for each case, resulting in 4 s of data. An analysis of the far-field acoustic spectra found this length to be sufficient for statistical convergence.

The far-field acoustic pressure is acquired at three polar angles: 30, 60, and 90 deg, as measured from the downstream jet axis. The radial distance of the microphones ranges from 101D at 30 deg to 145D at 60 deg. The near-field pressure was acquired using a linear array of 16 microphones located along the meridional plane of the jet; the spacing varied along the array from 1D to 2D (Fig. 2b). The linear

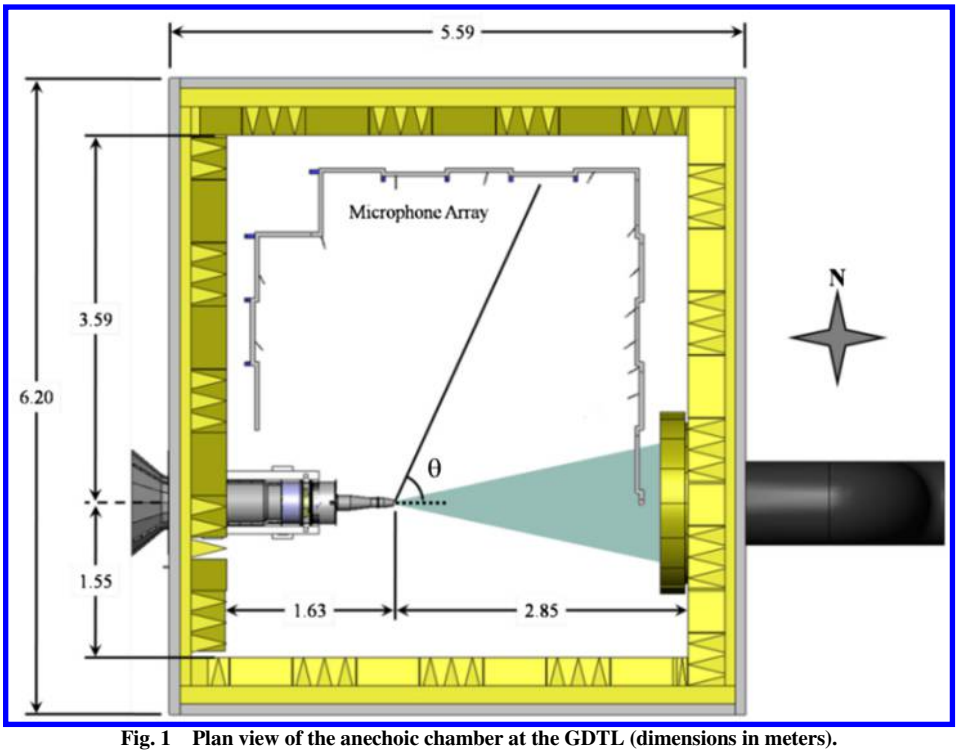

Fig. 1 Plan view of the anechoic chamber at the GDTL (dimensions in meters).

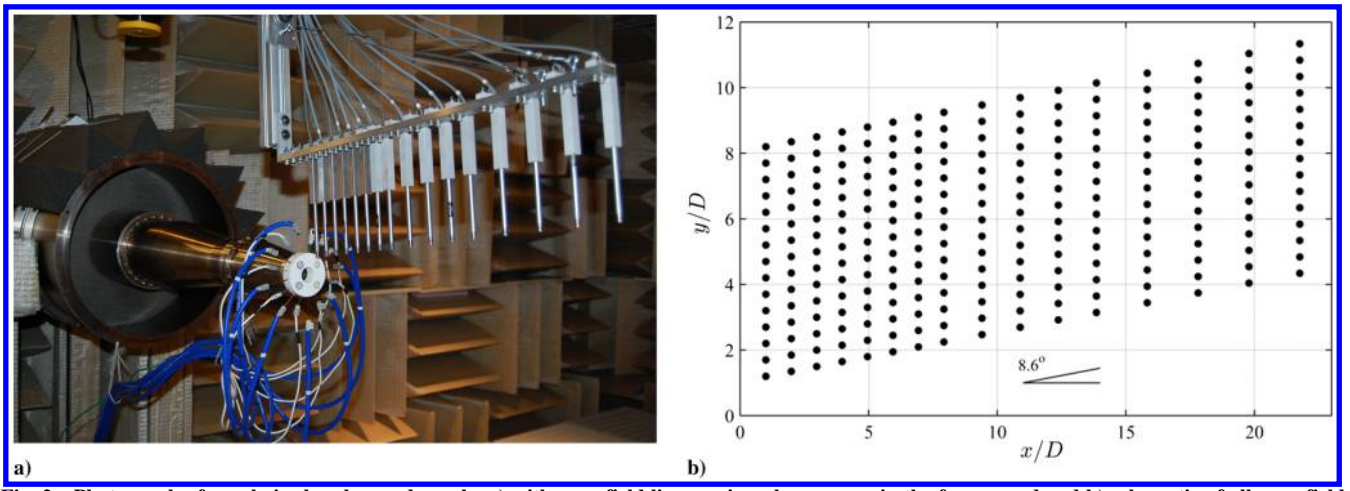

Fig. 2 Photograph of anechoic chamber and nozzle, a) with near-field linear microphone array in the foreground and b) schematic of all near-field microphone locations.

array is mounted on a linear traverse system at an angle of 8.6 deg to the jet axis to match the spreading angle of the jet shear layer for this Mach number, as determined via particle image velocimetry (PIV) measurements during previous studies [28]. The traverse is controlled using LabVIEW, and enables the acquisition of pressure measurements at various radial positions with respect to the jet axis. Initially, the most upstream microphone is positioned at $x/D = 1$ and $r/D = 1.20$, to ensure that the microphone tips are outside the mixing layer and do not affect the flowfield. For subsequent cases, the microphone array is incremented radially outward by $0.5D$ for a total travel distance of $7D$. A schematic of the microphone locations can be found in Fig. 2b.

In the present work, the phase-averaging technique used by Sinha et al. [26] is employed to study the evolution of the seeded perturbations, both spatially and temporally. The transistor–transistor logic (TTL) pulse sequence, which controls the LAFPAs, is supplied to an Agilent 33220A waveform generator. The rising edge of the TTL pulse triggers a sharp drop in the output voltage of the waveform generator, which then ramps back up to the original voltage over a time interval, which is shorter than the minimum excitation period. The output from the waveform generator is acquired simultaneously with the near- and far-field pressure signals using the aforementioned National Instruments hardware and software. As the excitation frequency, azimuthal mode, and ramp signal are well defined, this system enables the identification of the zero phase of actuation, and hence, the ability to phase average the pressure signals over the excitation period.

An analysis of the near-field response of the forced jet is not immediately straightforward due to acoustic contamination from the actuators themselves [26]. LAFPAs operate on a joule-heating principle — the breakdown of the air between the electrodes and the ensuing flow of current results in intense heating of the air. This rapid, localized thermal perturbation produces a compression wave, which excites the shear layer. However, this compression wave is still evident as it travels through the near field. Obviously, this is an undesirable effect, as this actuator self-noise may, in some cases, obscure the hydrodynamic and acoustic response of the jet.

In the present work, the near-field pressure signals have been preprocessed using a continuous-wavelet-based filtering algorithm, which has been specifically designed to remove the actuator self-noise while leaving the signature of the jet response unaltered. An example of this filtering can be found in Fig. 3, in which the original and filtered signals have been plotted for $St_{\mathrm{DF}} = 0.02$ at $x/D = 1$, $y/D = 1.20$. To aid in visualization, the results for multiple excitation periods have been phase averaged to produce these waveforms; the time-of-arrival of the actuator self-noise is predicted by the triangular marker. For consistency with other studies, the pressure in the current study has been normalized by the jet dynamic head, $p^* = p/\rho U_j^2$. As the actuator self-noise is localized in both time and frequency, and can be well predicted, a smoothing algorithm in the wavelet domain was found to be the most effective method for removing the undesirable noise while leaving the response of the jet intact. A fourth-order Paul wavelet is employed, due to the similarity of its imaginary component to the phase-averaged response of the jet. The energy of the response of the jet is well defined in the wavelet domain, with the actuator self-noise existing as high-frequency, temporally localized oscillations superimposed on this field. After smoothing in the wavelet domain to remove these oscillations, the signal is transformed back into the physical domain where it undergoes another smoothing operation to remove small-amplitude high-frequency oscillations, which may be introduced by the wavelet smoothing. Hereafter, all results examined within this work have been computed from the preprocessed, rather than the raw, signals.

C. Wave-Number/Frequency Filtering

The irrotational near field of the jet comprises both the hydrodynamic footprint of the large-scale structures in the mixing layer as well as the acoustic radiation. As has been discussed by numerous other researchers, interpretation of the near-field pressure is hampered by the inherent ambiguity regarding what fluid phenomena are being measured. A recent analysis [11,30] has shown that the total near field can be thought of as a linear superposition of these two constitutive fields. Therefore, a suitably designed linear filter can, in principle, extract the constitutive fields from the experimentally measured near field.

In this work, the decomposition is obtained via a Fourier-based wave-number/frequency filtering operation computed separately along the microphone array at each radial position. Fundamentally, the approach used in the present work is similar to that of Tinney and Jordan [12]. For the jet Mach number explored in this study, all hydrodynamic components are expected to have a subsonic convection velocity aligned in the axial direction. In contrast, acoustic fluctuations will appear either sonic or supersonic along the microphone array, depending on the source location. Hence, the decomposition can be accomplished by setting the filter cutoff based on axial wave number, $k_a = \omega/a_\infty$, at each frequency, and additional Fourier transforms in space are unnecessary [12].

This distinction of phase velocity for the different energy components can be observed in Fig. 4, in which the energy content in frequency/wave-number space has been plotted for the third radial microphone-array position. The sonic line has been overlain on the plot; energies below this line correspond to subsonic waves and above this line supersonic. Owing to the close proximity of the microphone array to the jet shear layer, the dominant pressure fluctuations are hydrodynamic in nature [31]. As can be seen in the figure, the dominant-energy region lies below the sonic line, corresponding to subsonically convecting waves, as we would expect. Although not readily apparent at low frequencies and low wave numbers (near the dominant-energy-containing region), at high frequencies and high wave numbers two distinct energy lobes

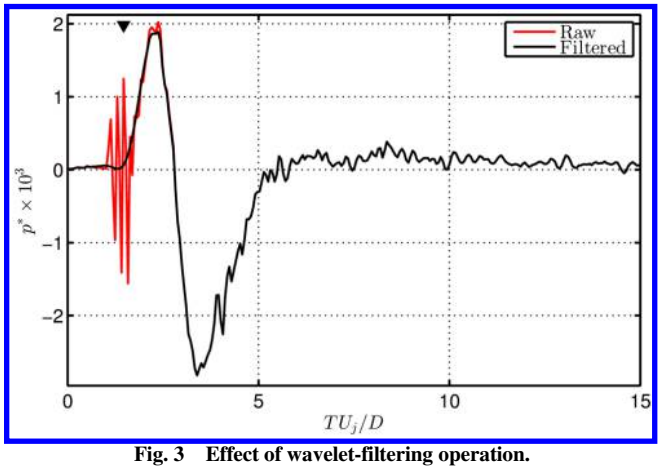

Fig. 3 Effect of wavelet-filtering operation.

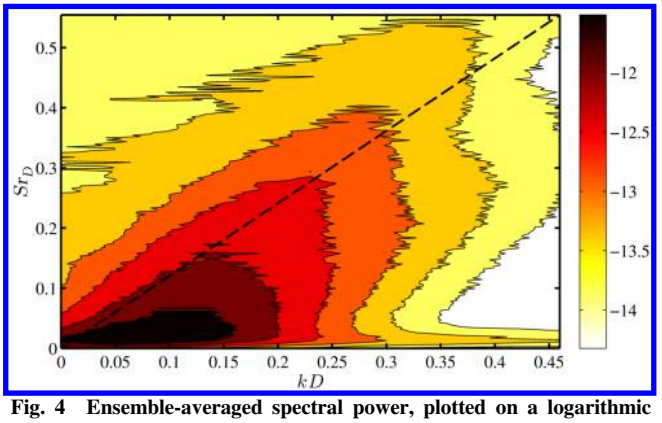

Fig. 4 Ensemble-averaged spectral power, plotted on a logarithmic scale; the acoustic velocity of the ambient air is denoted by the dashed line.

become apparent: one subsonic, corresponding to the convective signature of the large-scale structures, and one supersonic, corresponding to the generated acoustic radiation. That the acoustic-energy lobe occurs in the supersonic regime, rather than centered about the sonic line, is due to the oblique impingement of the acoustic waves upon the linear microphone array. These results confirm the applicability of the wave-number/frequency filter to decompose the total near-field pressure into its acoustic and hydrodynamic components.

Therefore, the transformed pressure field is computed as

$$\hat{p}(k_x, \omega) = \iint W_w(x,t)\, p(x,t) e^{-i(\omega t - k_x x)}\, \mathrm{d}x\, \mathrm{d}t$$

Note that the realities of the physical setup require the transform to actually be computed along the microphone-array angle, which is inclined slightly with respect to the jet axis; it is from this wave number that the axial wave number is then computed. The window function W_w is defined as a Tukey window to minimize the spectral-leakage effects, as well as distortions to the original signal after the subsequent inverse transforms; the Tukey window, or equivalent-type windows, has been used by previous researchers for similar-type applications [12,32]. To ease in computation of the discrete Fourier transform (DFT), the experimental data are interpolated onto a regular grid of spacing $1D$ using a cubic spline. The subsonic and supersonic components are then computed separately as

$$p_c(x,t) = \frac{1}{(2\pi)^2} \iint \boldsymbol{W}_c(k_x, \omega) \hat{p}(k_x, \omega) e^{i(\omega t - k_x x)}\, \mathrm{d}k_x\, \mathrm{d}\omega$$

in which the component weight vector, $\boldsymbol{W}_c \in [0, 1]$, is set based on the phase velocity for each k_x, ω pair.

Because of the discrete nature of the Fourier transform being performed, an exponential decay about the sonic wave number is used, rather than a sharp cutoff. This reduces the effects of the windowing (specifically, energy leakage) and decreases ringing in the decomposed waveforms, which is caused by Gibbs phenomenon. An example of this can be found in Fig. 5, in which the power spectral density (PSD) at a single microphone has been plotted for the signals decomposed with the sharp and exponential-decay cutoffs. The use of the sharp cutoff was found to produce nonphysical oscillations in the decomposed spectra. By shifting to an exponential decay, which recaptures some of the energy that inevitably leaks across the sonic boundary, these oscillations are damped and physically realistic spectra emerge. The width of the exponential decay is unfortunately a free parameter that must be set by the researcher. In this work, the minimum width (i.e., sharpest cutoff), which produced smooth spectra in the unforced jet, was used for all cases; the purpose of this was to recapture the energy that has leaked over the sonic line while minimizing the amount of energy included that truly belongs on the other side of the sonic boundary; this value was found to be $\sim 0.74 dk_x$. In some cases, the use of the sharp exponential decay results in small quantitative changes in the results. An example of this can also be found in Fig. 5, in which the excitation tonal amplitudes in the acoustic spectra have been amplified by the change in cutoff width. A parametric study of the effects of the cutoff sharpness (as well as the forward transform window) was conducted to ensure that the final conclusions remain unaffected. More recently, validation of the Fourier-based, EMD-based, and a newly proposed wavelet-based decomposition algorithm was performed using the current experimental database; results from this validation can be found in Crawley and Samimy [33]. The wavelet-based decomposition method was found to eliminate ringing in the decomposed signals, as well as extracting temporally localized acoustic events. However, for the purposes of the current study, the much simpler Fourier-based method was deemed sufficiently accurate.

III. Results

The identification of the source dynamics first requires a thorough examination of the hydrodynamic response of the jet to excitation. This will be accomplished by an investigation of the evolution of the phase-averaged waveforms in space, and the quasi-linear model of Sinha et al. [26] will be evaluated. Following this, the dominant acoustic-source region will be identified, in an approximate sense, by identification of the radiated energy from the near field to the far field computed via two-point correlations. Subsequently, the near-field pressure will be decomposed into its constitutive acoustic and hydrodynamic fields using the wave-number/frequency filter. These decomposed fields will be investigated using phase averaging and two-point correlations as well. Finally, details of the noise-generation process, namely, temporal coherence, will be explored using wavelet transforms.

A. Response of the Irrotational Near Field of the Jet

1. *Quasi-Linear Response to Excitation*

Sinha et al. [26] studied the irrotational near-field response of a subsonic jet subjected to excitation with plasma actuators by decomposing the instantaneous fluctuating pressure field into a coherent wave component (which corresponds to the large-scale structure generated by the excitation) and incoherent residual fluctuations (which correspond to the natural turbulence in the jet). Fundamentally, this decomposition is similar to the triple decomposition used by Hussain and Reynolds [34]. Sinha et al. [26] found that each pulse from the actuators produces a coherent large-scale structure that would grow, saturate, and decay as it advects through the jet shear layer. In the irrotational near field, the signature of these large-scale structures takes the form of a compact waveform. At low-enough excitation frequencies, the characteristic period of this waveform is much less than the excitation period, and hence, the

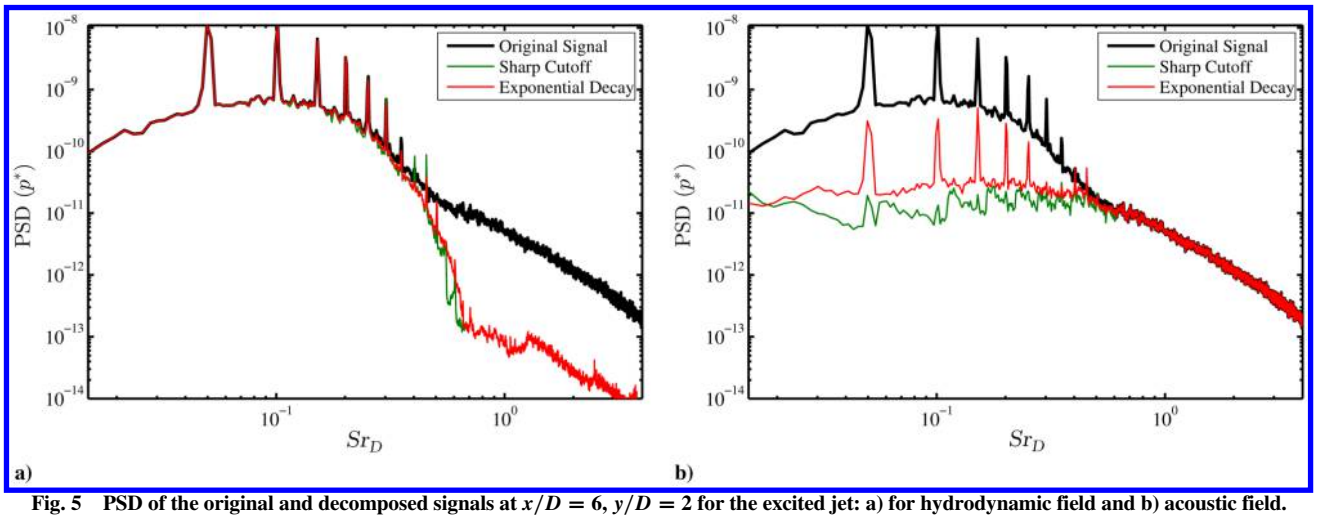

Fig. 5 PSD of the original and decomposed signals at $x/D = 6$, $y/D = 2$ for the excited jet: a) for hydrodynamic field and b) acoustic field.

structures seeded by the excitation do not interact with one another as they evolve downstream. Therefore, their behavior can be thought of as representing the response of the jet to a single perturbation; in short, this is the impulse response of the jet, which is produced by the impulsive excitation by LAFPAs [16].

As the excitation frequency is increased, the excitation period will decrease to the point where the characteristic period of the impulse response is on the same order as, or greater than, the excitation period. In this excitation regime, the large-scale structures are no longer evolving independently. As the period of actuation approaches the characteristic period of the impulse response, the waveforms extracted by the phase-averaging technique are largely unmodified from that of the impulse response. Above this frequency, a significant interaction between the structures is observed, with noticeable modifications to the waveform shape and amplitude. As the structures are growing as they advect through the shear layer, the frequency at which the structures begin to interact is dependent on the axial location.

This behavior of independent evolution and periodic interactions between structures can be observed in Fig. 6, in which the phase-averaged response of the jet has been plotted along the first microphone-array position (closest to the jet shear layer) at two axial locations, $x/D = 3$ and $x/D = 6$, for all St_{DF} explored in this study (except $St_{DF} = 0.05$, which has characteristics similar to that of 0.02). At the upstream position, the impulse response of the jet is observed at the two lowest excitation frequencies, $St_{DF} = 0.02$ and 0.05 (not shown here), as the characteristic period of the compression and expansion waves is much less than the period of excitation. For $St_{DF} = 0.15$–0.25, the waveform magnitudes and shape are largely unaffected; yet, the characteristic period of the response is reduced due to the structure interactions. Further increases in the excitation frequency, to $St_{DF} = 0.35$ and 0.50, yield structures for which the amplitude has been significantly reduced, as has the characteristic period. Further downstream, the frequencies at which structure interactions occur have shifted due to the growth of the coherent structures.

It was shown [26] that, for a certain range of excitation frequencies ($St_{DF} \leq 0.50$ at $x/D = 2$, for example), the structures interact in a quasi-linear manner, insofar as their near-field pressure signatures are concerned. To be precise, the response of the jet in the irrotational near field could be well predicted by a linear summation of the impulse response of the jet, repeated at the periodic excitation frequency. This concept has been illustrated in Fig. 7, in which the periodic response of the jet to excitation with $St_{DF} = 0.50$ has been reproduced at $x/D = 3$ and $x/D = 8$. Additionally, a linear superposition of the impulse response for $St_{DF} = 0.05$, repeated to match the excitation frequency of $St_{DF} = 0.50$, has been overlaid. The linear superposition has been arbitrarily shifted in time to match

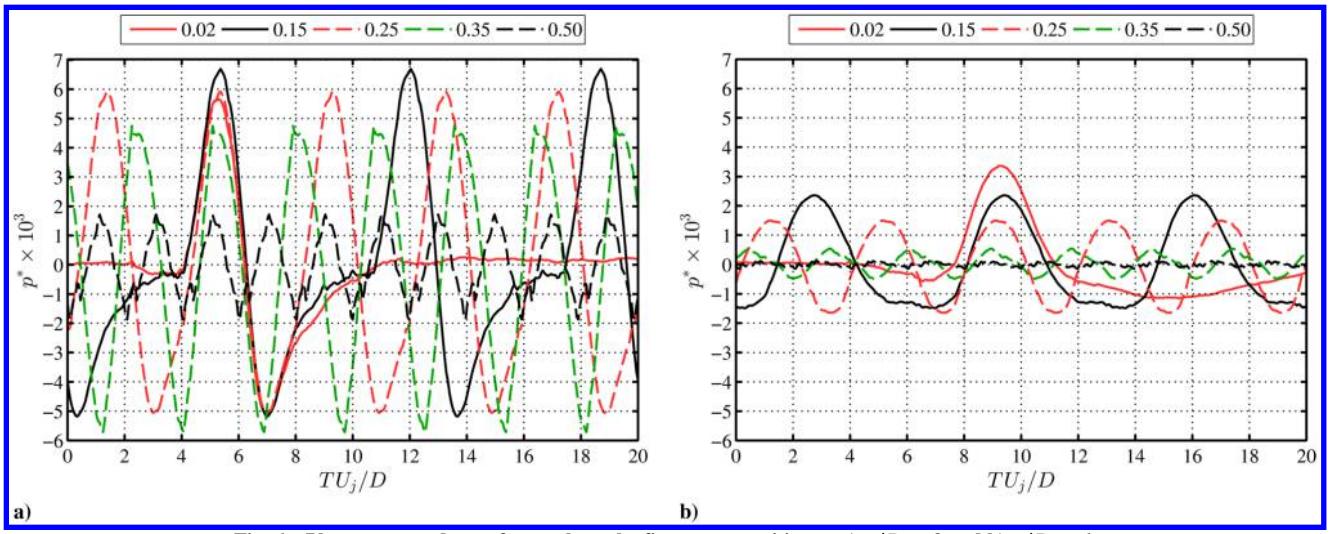

Fig. 6 Phase-averaged waveforms along the first array position at a) $x/D = 3$ and b) $x/D = 6$.

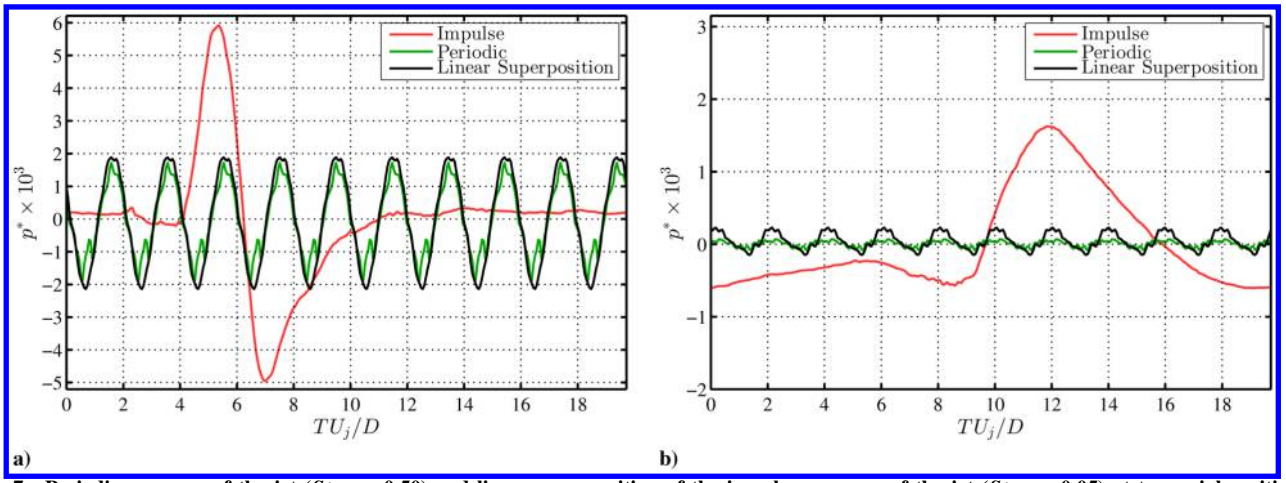

Fig. 7 Periodic response of the jet ($St_{DF} = 0.50$) and linear superposition of the impulse response of the jet ($St_{DF} = 0.05$) at two axial positions: a) $x/D = 3$ and b) $x/D = 8$.

the phase of the periodic response; this phase difference is likely due to the dependence of convection velocities on structure frequency [35] (or more accurately, structure size). For reference, the impulse response has also been included in the plots. Upstream of the end of the potential core ($x/D = 6$, as determined previously in our facility by PIV [28]), the quasi-linear interaction model produces close predictions of the waveform amplitude and shape, despite the significant difference in both peak amplitude and waveform shape between the impulse and periodic responses.

The accuracy of the model is reduced as the excitation frequency is increased or as the probe is traversed downstream. At $x/D = 8$, for example, the linear superposition waveform matches the period of the periodic response, but drastically overpredicts the amplitude of the compression wave. There are several likely sources for the discrepancies between the linear superposition and the periodic responses of the jet. As discussed by Sinha et al. [26], nonlinearity in the structure-interaction dynamics is one obvious source. Another possible cause is the structure-advection dynamics, which will be investigated in subsequent sections. Basically, if there is a structure scale (or inversely, frequency) dependence on the axial location at which coherent structures collapse, the linear superposition model is no longer applicable at these locations.

This quasi-linear interaction of the jet response to excitation is not limited exclusively to the hydrodynamically dominated regions of the jet, but, in fact, holds for the acoustic far field as well, at aft angles (where the acoustic signal is strongest and is known to correlate well with large-scale structures). This can be observed in Fig. 8, in which the phase-averaged response of the jet in the acoustic far field at a polar angle of 30 deg has been plotted. For legibility, only a select number of excitation Strouhal numbers have been included. As with the irrotational near field, the acoustic far field exhibits a compact waveform for the lowest excitation Strouhal numbers. (The response for $St_{DF} = 0.05$ was virtually identical to $St_{DF} = 0.02$.) Although nearly a direct inverse from the waveform observed in the hydrodynamically dominated near field, the far-field waveform is quite reminiscent of the phase-averaged waveforms observed by Kambe and Minota [36] for the acoustic radiation toward aft angles produced by the head-on collision of vortex rings. For $St_{DF} = 0.15$ and 0.25, the primary expansion and compression waves remain nearly unchanged from the fundamental response. However, at higher St_{DF}, a continuous oscillation between sharp expansion and compression waves is again observed, although both the amplitude and period are reduced from the impulse response. As before, a linear superposition of the impulse response can well predict the waveform shape and amplitude at the higher excitation frequencies, although in this case, only up to $St_{DF} = 0.25$. Whether this breakdown in the linear superposition model at the highest excitation frequencies is due to nonlinear behavior or uncertainty in the phase averaging is currently unknown. The phase-averaged waveforms were also investigated at polar angles of 60 and 90 deg; however, a clear waveform was not identifiable over the statistical uncertainty inherent in the phase-averaging process (likely due to the superdirective character of the acoustic radiation [7], which renders the amplitude at sideline angles too low to be detectable).

2. *Structure-Advection Dynamics*

To better understand the relationship between the near-field dynamics and the acoustic radiation reaching the far field, two-point correlations were computed (using the measured signals, as opposed to the phase-averaged waveforms) between each microphone in the near field and the far-field microphone at 30 deg. The correlations were then examined in the spatiotemporal domain, which showed distinct regions of positive and negative correlations spanning several jet diameters and flow timescales. The physical phenomena to which these correlation regions correspond can be determined with the help of expected times of arrival. Two such times of arrival are sketched in Fig. 9; conceptually, these are identical to those of Bogey and Bailly [37], although our probe locations are outside the jet shear layer. The first expected time of arrival, τ_{ac}, corresponds to the expected time lag for an acoustic wave traveling directly from the noise source to the near-field microphone and on to the far-field microphone. The second, τ_{con}, corresponds to the expected time lag for a large-scale structure to convect to the acoustic-source region from the near-field microphone's axial station, generate noise, and radiate acoustically to the far-field microphone. For simplicity, the density and convection effects on the acoustic wave as it travels through the jet shear layer have been neglected in this analysis. By necessity, it has been assumed that the acoustic radiation in the jet is dominated by $m = 0$ azimuthal Fourier mode. (The near-field and far-field microphone arrays are not at the same azimuthal angle with respect to the nozzle.)

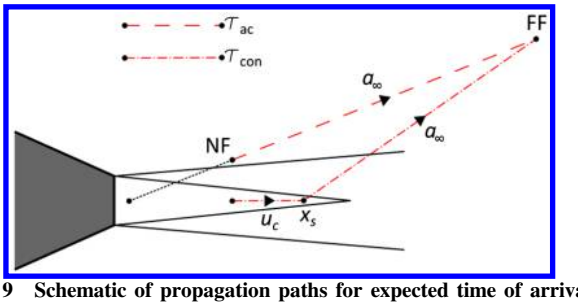

Fig. 9 Schematic of propagation paths for expected time of arrivals between near-field microphone (NF) and far-field microphone (FF) (not to scale).

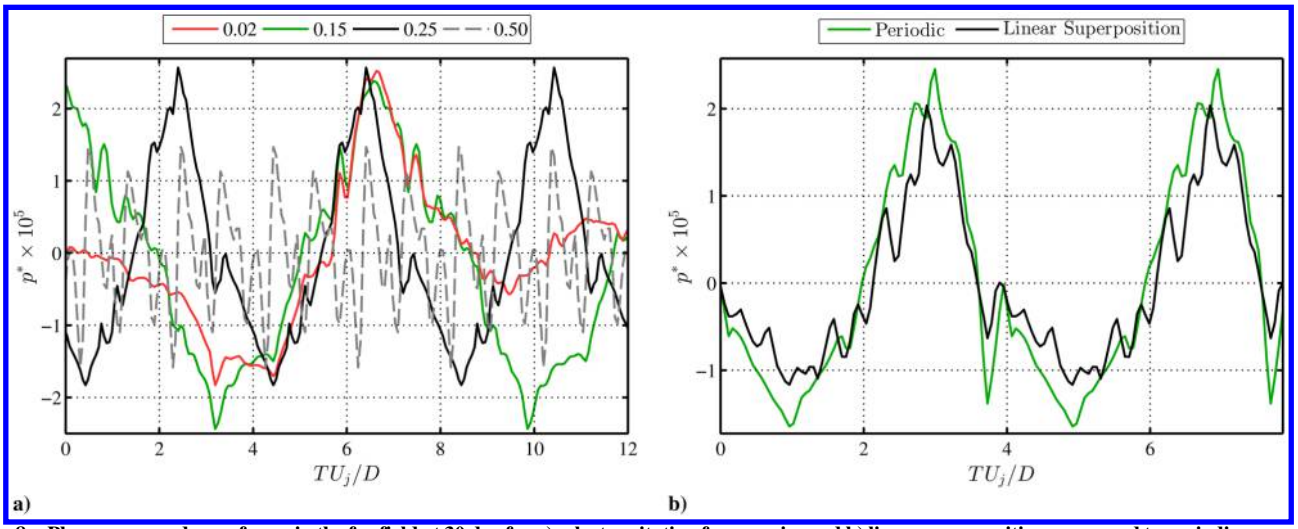

Fig. 8 Phase-averaged waveforms in the far field at 30 deg for a) select excitation frequencies and b) linear superposition compared to periodic response at $St_{DF} = 0.25$.

This assumption is easily justified in the excited jets, where the actuators have been fired in phase. While the near-field pressure and acoustic radiation toward aft polar angles in a natural, high-Reynolds-number jet are a combination of numerous azimuthal Fourier modes, previous researchers have found these fields to be dominated by the axisymmetric mode [10,38–40]. The convection velocity was held constant for these estimations at $U_c/U_j = 0.69$. This value was obtained by performing two-point correlations between all adjacent microphones located in the most upstream region of the jet ($x/D \leq 5$, before the end of the potential core), and then averaged. The acoustic-source region was assumed to be $x_s/D = 4$. (This value was chosen to best match the observations made subsequently.) It should be noted that this analysis method is not meant to suggest that the noise-generation process occurs at a specific point in space, but that the source region primarily exists (in a time-averaged sense) around $x/D = 4$.

The correlations from the near field to the far field at 30 deg can be found in Fig. 10 for the unforced jet, along two array positions The expected times of arrival, τ_{ac} and τ_{con}, have been denoted in the figure by the solid and dashed lines, respectively. To aid in identifying the physical phenomena to which the correlation regions correspond, the time lag τ in the figures has been nondimensionalized by the ambient speed of sound a_∞ and R, the distance from each near-field microphone to the far-field microphone. (Note that this results in an ordinate that is scaled separately along the abscissa, due to the dependence of the axial position on R.) Near the jet shear layer, four distinct correlation regions can be observed: two positive, two negative; one strong and one weak for each. The first correlation regions, the strong negative and weak positive, are noticeable beginning at the most upstream microphone, and reach their peak values around $5 < x/D < 10$, decaying significantly beyond that. The slopes of these regions indicate propagation velocities below the sonic velocity; in the upstream region, they roughly match with the measured convective velocity of the large-scale structures, and they gradually decrease beyond the potential core, as expected. Conversely, the strong-positive and weak-negative correlation regions exhibit propagation velocities that match well with the ambient speed of sound. These correlation regions start from almost negligible values upstream, strongly amplify near and just beyond the end of the potential core, and decay gradually in the most downstream region.

As the microphone array is moved radially outward, the strong-negative and weak-positive correlation regions quickly decay to negligible values. By $y/D = 4.20$, all observable correlation regions match the expected time of arrival for an acoustic wave, and are of significantly greater amplitude. The distinctly different propagation velocities and axial and radial evolutions of the two pairs of correlation regions indicate that these correspond to different physical phenomena. The strong-negative and weak-positive correlation regions observed near the jet shear layer likely are associated with the large-scale structures themselves, rather than the acoustic phenomena. The positive and negative correlation regions are likely associated with the braid and core regions of the large-scale structure as they convect through the shear layer. The low-pressure core region of the vortex produces a positive correlation value with the far-field acoustic due to the phase inversion of the acoustic waveform at low polar angles (Fig. 8). At this radial location, the dominant energy measured by the microphone array is acoustic, owing to the strong decay of the hydrodynamic field with radial distance from the jet.

Similar correlation regions between the near field and far field at 30 deg can be found in the case of the excited jets (Fig. 11). In the impulse-forced jets ($St_{DF} = 0.02$, Fig. 11a), four distinct correlation regions are again observed, as with the unforced jet. As before, the strong-positive and weak-negative correlation regions exhibit propagation velocities matching the sonic velocity in the downstream region. However, the strong-positive region no longer shows negligible correlation in the upstream region, instead exhibiting moderate correlation values and a change in slope to match the convective velocity of the large-scale structures rather than the sonic velocity. As will be discussed shortly, the structures generated by the excitation, and the dynamics of which in turn generate acoustic radiation, are more coherent and energetic than the naturally occurring structures.

Increasing the excitation frequency to $St_{DF} = 0.15$ results in one distinct positive and negative correlation region produced per excitation period. As was discussed in the previous section, increasing the excitation frequency, such that the characteristic period of the structures is roughly equal to the excitation period, results in quasi-linear interactions and roughly periodic waveforms (see Figs. 6 and 8). With this behavior in mind, the periodic behavior of the correlation field is unsurprising. For both positive and negative regions, the maximum correlation is found to be located near the end of the potential core, at $4 < x/D < 6$. In the upstream region, the correlations match the convective velocity and have been greatly enhanced in strength; for $x/D > \sim 8$, a marked decay is observed coinciding with a shift in propagation velocity to match the sonic velocity. In the downstream region, continuously oscillating positive and negative correlation regions with sonic propagation velocities are also found, although one particular region, corresponding to the expected time of arrival for an acoustic wave traveling directly from the near-field microphone to the far-field microphone, is dominant over the rest. It should be noted that the positive correlation region in the upstream that merges with this particular correlation region in the downstream matches not just the convective velocity for the large-scale structures, but the expected time of arrival for a source that is producing acoustic radiation around the assumed source location, $x_s/D = 4$.

As the excitation frequency is further increased, the region over which strong, periodic correlations with convective velocities occur decreases, from $x/D < \sim 8$ at $St_{DF} = 0.15$ to $x/D < \sim 5$ at $St_{DF} = 0.25$, as does the amplitude of the correlations. This also

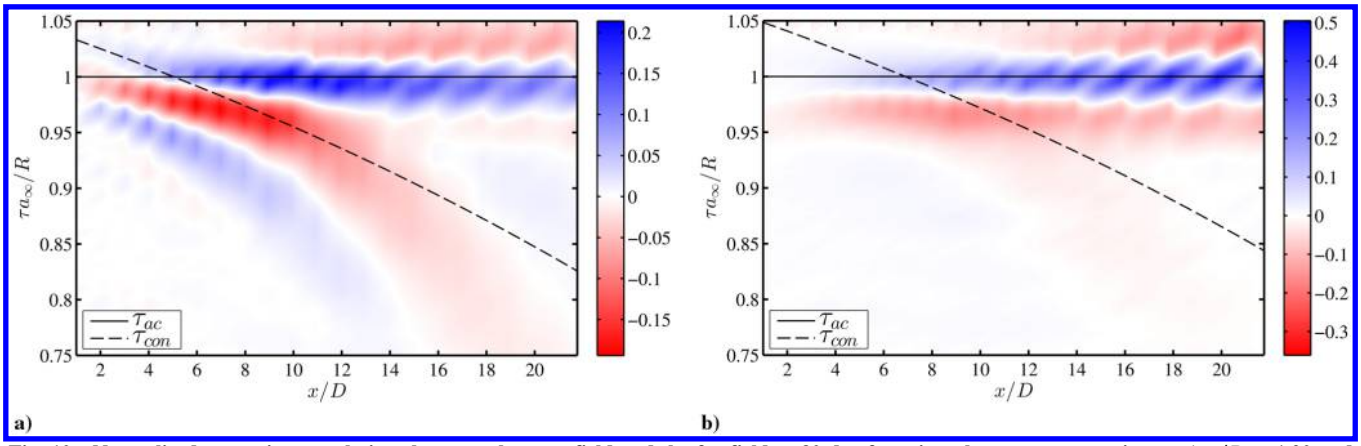

Fig. 10 Normalized two-point correlations between the near field and the far field at 30 deg for microphone arrays starting at a) $y/D = 1.20$ and b) $y/D = 4.20$.

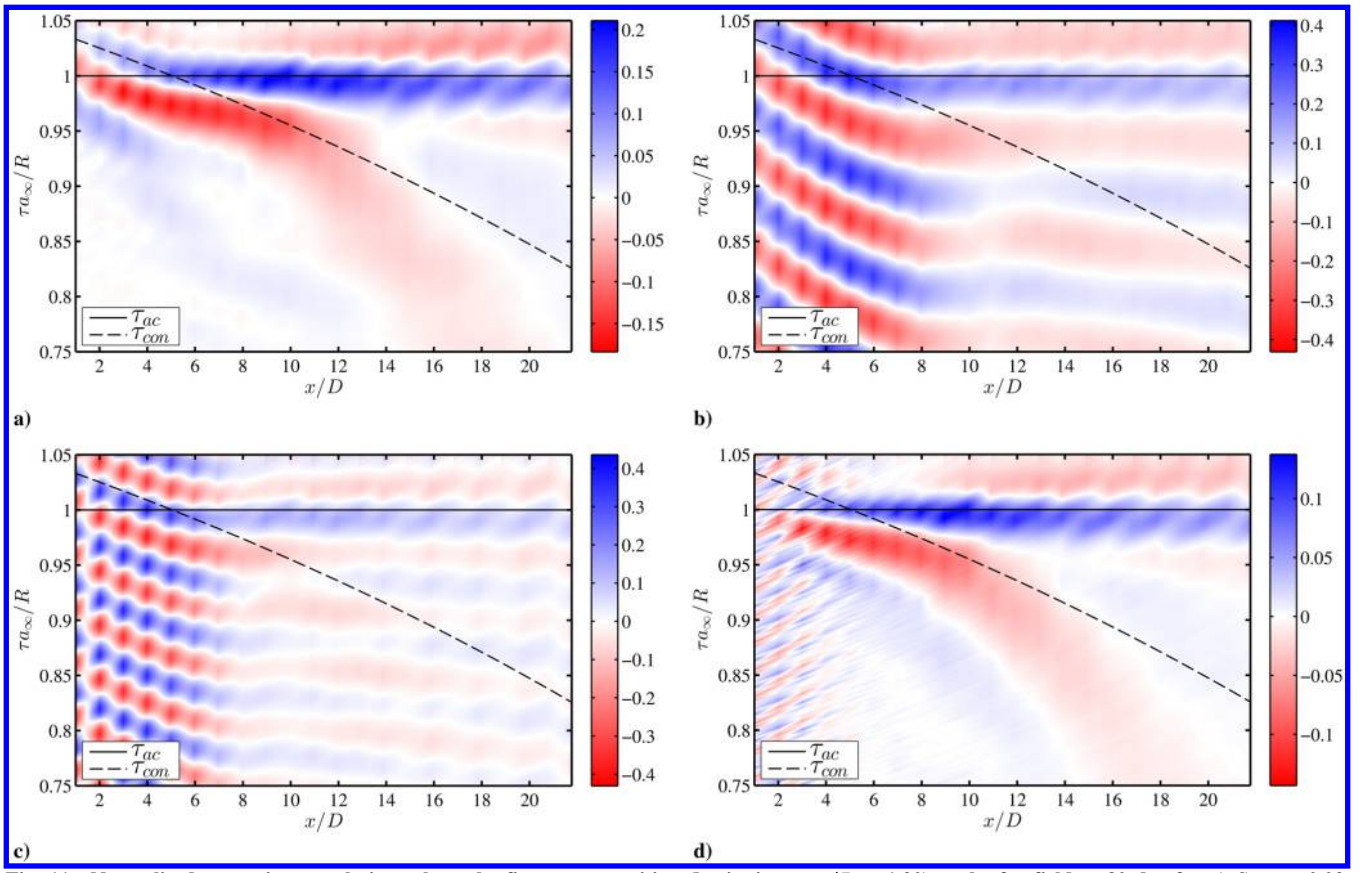

Fig. 11 Normalized two-point correlations along the first array position (beginning at $y/D = 1.20$) to the far field at 30 deg for a) $St_{DF} = 0.02$, b) $St_{DF} = 0.15$, c) $St_{DF} = 0.25$, and d) $St_{DF} = 0.50$.

corresponds to a slight upstream shift in the apparent source region. By $St_{DF} = 0.50$, the correlation regions have nearly returned to the baseline state, indicating that the structures generated by the excitation at this frequency are no longer the dominant sources of noise in this jet.

The slight upstream shift in the apparent source region can be interpreted in light of the growth, saturation, and decay of the large-scale structures generated by excitation as they convect downstream. This is illustrated in Fig. 12, in which the mean square of the pressure fluctuations has been plotted along the first array position. In the case of the unforced jet, the fluctuations peak at $x/D = 5$, just upstream of the end of the potential core, and slowly decays beyond that point. Excitation at the lowest frequencies, where the structures do not undergo significant quasi-linear interactions (per Fig. 6), results in an amplification of the fluctuation energy over nearly the entire domain, although it is most significant near the saturation point. In this case, the saturation point has shifted upstream, to $x/D = 4$, and displays a slightly sharper peak. Increasing the excitation frequency yields further amplification of the pressure fluctuations, as well as an upstream shift in the saturation location. These results are consistent with those of other researchers, who have shown that perturbation of higher frequencies saturates earlier upstream than lower frequencies [41,42]. The change in peak amplitude is nonmonotonic with excitation frequency; the maximum amplification occurs for $St_{DF} = 0.25$–0.35, and decreases quickly for the highest excitation frequency. This corresponds to the well-documented jet-column-mode excitation response [4].

The overall similarities between the correlation regions for the unforced and forced jets at a range of frequencies are highly suggestive of a consistent source mechanism (or mechanisms) for all of the jets. The trends observed in these figures are indicative of coherent structures, which convect through the shear layer in the jet core region and primarily emit acoustic radiation near the end of the potential core. A similar behavior has been observed computationally [37]. It remains to be seen, however, if the location where the dominant downstream and upstream positive correlation regions merge indicates the beginning of the source region, or if the acoustic radiation from the large-scale structures exists in the most upstream region and it is being masked by the correlations to the large-scale structures. This will be investigated by decomposing the total near-field pressure into its constitutive hydrodynamic and acoustic components, and analyzing each component separately.

B. Response of the Decomposed Fields

Subsequent to the wave-number/frequency filtering (Sec. II.C), the separate hydrodynamic and acoustic fields can be reanalyzed akin to the full signals. The DFT inherent in the wave-number/frequency

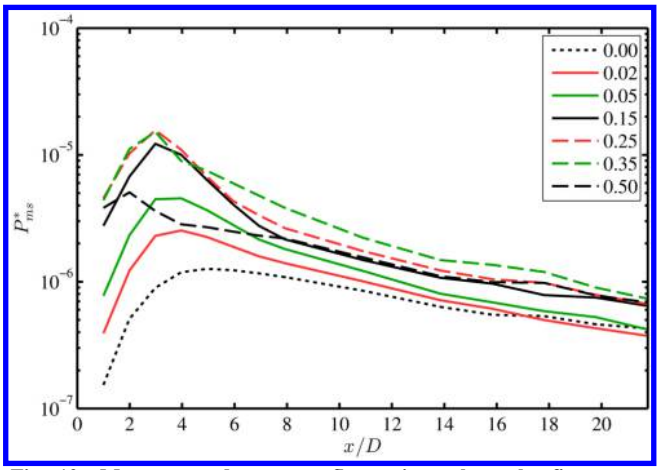

Fig. 12 Mean-squared pressure fluctuations along the first array position; the unforced jet is indicated as 0.00.

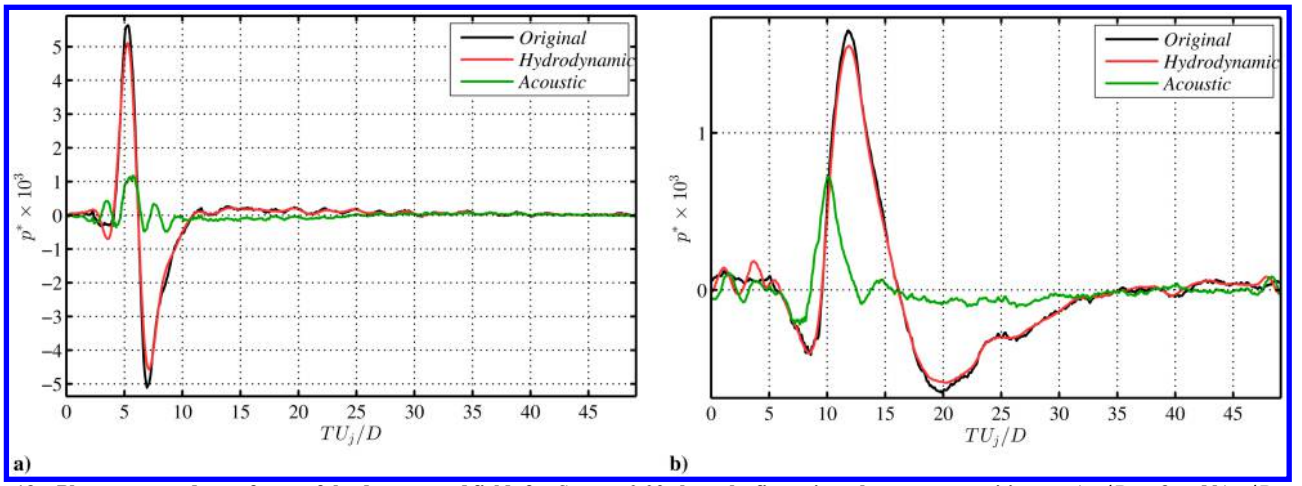

Fig. 13 Phase-averaged waveforms of the decomposed fields for $St_{DF} = 0.02$ along the first microphone-array position at: a) $x/D = 3$ and b) $x/D = 8$.

filtering necessitates the application of a window function (to minimize spectral leakage) to the original waveforms before the forward transform. An unfortunate effect of this is the corruption of the reconstructed waveforms near the spatial boundaries; hence, these locations are not included in the following analysis.

1. *Wave Response*

The phase-averaged waveforms for $St_{DF} = 0.02$ are shown in Fig. 13, in which the original and decomposed fields have been plotted for two axial positions, $x/D = 3$ and $x/D = 8$, along the first array position. In both cases, the hydrodynamic waveform closely matches the original waveform, which is unsurprising given the proximity of the microphone array to the jet shear layer. Distinct acoustic fluctuations are observed at all axial positions, however, which have a characteristic shape that is fundamentally different from the original and hydrodynamic waveforms. These acoustic fluctuations do not match the shape, amplitude, or phase of the actuator self-noise, which should be filtered out of the original signals before the wave-number/frequency filtering, per Sec. II.C. In the upstream position, the acoustic waveform exhibits multiple compression and expansion waves, and is of much lower amplitude than the hydrodynamic. At this location, both waveforms represent an impulse response, in which the jet returns to its natural state long before the next excitation period. In the downstream location, the acoustic waveform has evolved to one in which a dominant expansion wave is trailed by a dominant compression wave. The acoustic response found here at the downstream position compares well with the waveform found at the far-field aft angles (Fig. 8) at this St_{DF}, which also exhibited an impulse response consisting of an expansion wave trailed by a compression wave.

Sample results for the response of the decomposed acoustic field over the range of excitation Strouhal numbers explored in this study can be found in Fig. 14. Coherent radiation over the entire spatial domain explored in this study is observed for all forced cases (not all shown). Because of the reduced excitation period at high St_{DF}, the response of the acoustic field is now periodic rather than impulsive. In the case of moderate excitation frequencies for which the generated structures are just beginning to linearly interact ($St_{DF} = 0.15$), the shape of the impulse acoustic response seen for $St_{DF} = 0.05$ is more or less retained, with one primary compression wave leading (or followed) by two smaller waves. Further increases in the excitation frequency to $St_{DF} = 0.25$ result in a significant alteration to the shape of the acoustic response. However, it can be shown that the waveform shape (if not the peak amplitude) can be well predicted by a linear superposition of the impulse acoustic response, similar to the results found in Sec. III.A for the total near field. In Fig. 14b, the impulse acoustic response to excitation ($St_{DF} = 0.02$) and the periodic response ($St_{DF} = 0.25$) has been plotted for $x/D = 6$. Additionally, a linear superposition of the impulse response repeated at the periodic frequency has been included. It is found that the linear superposition of the fundamental response matches the periodic response in shape and overall amplitude quite well, the only discrepancies being the

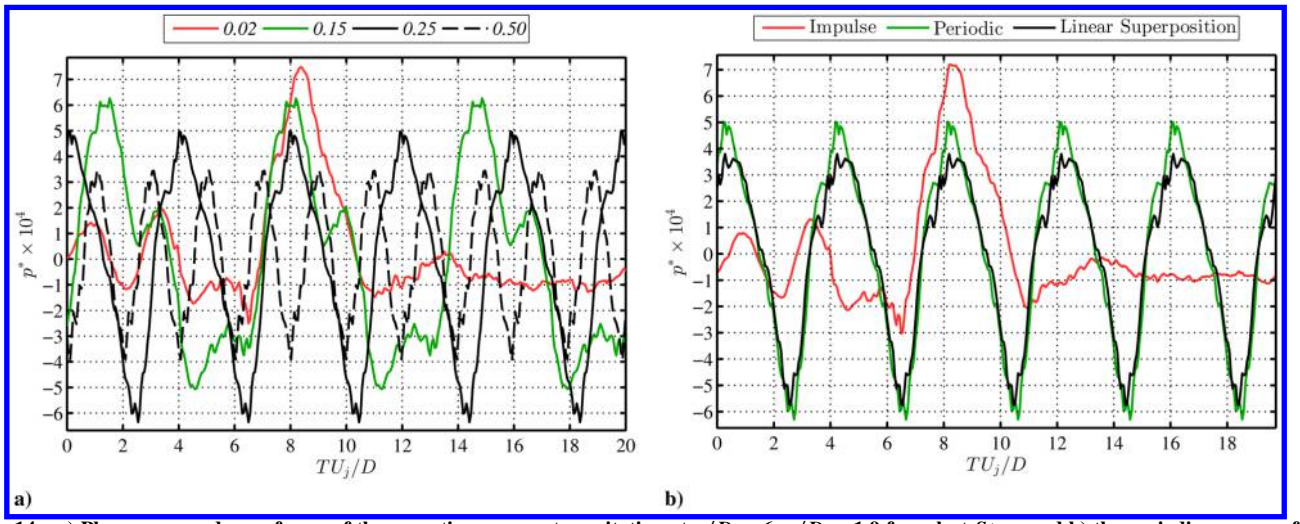

Fig. 14 a) Phase-averaged waveforms of the acoustic response to excitation at $x/D = 6$, $y/D = 1.9$ for select St_{DF}, and b) the periodic response for $St_{DF} = 0.25$ and a linear superposition of the impulse response.

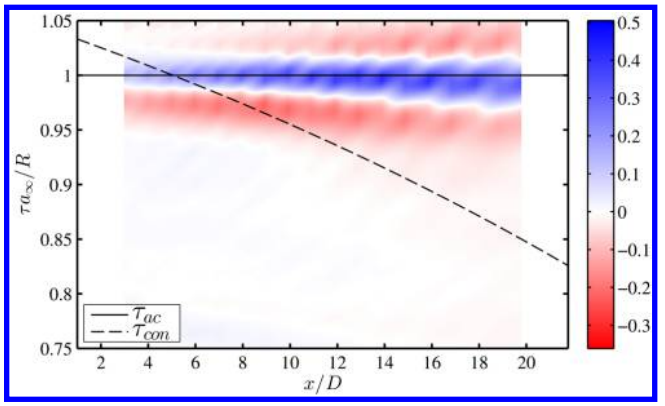

Fig. 15 Normalized correlations of the acoustic component in the unforced jet.

peak amplitude of the compression and expansion waves (a discrepancy that grows with increasing excitation Strouhal number). This strong similarity in the acoustic response to a broad range of excitation frequencies spanning the impulsive and periodic regimes indicates a consistent dominant-source mechanism for the large-scale structures.

2. *Acoustic-Source Region*

Experimental as well as theoretical results have shown that the acoustic sources in subsonic, unheated jets exhibit a quadrupolelike radiation pattern to the far field, with the primary radiation angle directed toward the aft angles, and the amplitude decaying exponentially with increasing polar angle. Nonetheless, acoustic propagation is spherical and centered on the source region, and hence, acoustic waves observed in the upstream region may, in fact, have their source in the downstream region. To investigate the source location for these acoustic waves (in an approximate sense), two-point correlations between the near field and far field at 30 deg were recomputed using only the acoustic component in the near field. As before, the two expected time lags, τ_{ac} and τ_{con}, have been overlain on the plots, and the abscissa has been normalized at each axial position by the ambient speed of sound and the distance from the near-field microphone to the far-field microphone. As with the phase-averaged waveforms for the decomposed fields, the correlations in the most upstream and downstream regions have been omitted due to boundary effects from the windowing and DFT.

The results shown in Fig. 15 correspond to the unforced jet along the first array position. A marked change in the upstream region is apparent when comparing these results against those for the full near field (Fig. 10a). No correlation regions matching the convective velocity of the large-scale structures exist; this confirms our previous assertion that the upstream correlation regions in Fig. 10 were associated with the large-scale structures themselves, rather than the direct acoustic phenomena. Instead, a single positive correlation region, roughly matching τ_{ac}, exists over the entire domain with a significantly enhanced correlation over the full-field results. In fact, the results found here for the acoustic component along the first microphone-array position are nearly identical to those for the full-field response at the further away array positions (Fig. 10b), which were dominated by acoustic, rather than hydrodynamic, energy.

Although initially overlooked, upon closer inspection, it becomes apparent that the positive correlation region does not line up exactly with τ_{ac}; the slight mismatch becomes progressively greater with downstream distance. This behavior can be seen more clearly in Fig. 16, in which the previous results have been replotted over a shorter period of time. As the near-field probes are located outside the source region, calculation of an expected time of arrival for an acoustic wave requires an assumption about the location of the source region. In formulating τ_{ac}, it was assumed that the source region lies directly on the line connecting the near-field microphone to the far-field microphone. Another expected time of arrival can be constructed by assuming the source region is stationary in space; from simple geometric considerations of the distance from the assumed source region to the near-field and far-field microphones, the time lag τ_s between the arrivals of an acoustic wave at both microphones can be computed. For the unforced jet, the acoustic source was assumed to be located at $x_s/D = 4$. (As before, this type of analysis is not meant to imply that the source region is located at a specific, fixed point — it is merely a convenient way of understanding the propagation paths.)

In the upstream region of the jet, the peaks of the positive correlation region match τ_{ac} nearly exactly. In the downstream region, τ_{ac} begins to increasingly overpredict the time lag for the maximum correlation. On the other hand, τ_s tracks the time lags for the peak correlation consistently over the downstream region, but not the upstream region. The results found here appear to indicate that the dominant acoustic radiation reaching the far-field aft angles is being generated over an extended region of the jet mixing layer, roughly $x/D \leq 4$ in the case of the unforced jet (although the correlations from the most upstream region are comparatively quite low). The authors would like to add several qualifications to this conclusion, however, as these results appear to contradict those of previous researchers who found the end of the potential core to be the dominant-source region in the jet (for example, Hileman et al. [43]). First, the linear microphone array cannot distinguish the radial or azimuthal position of sources, which will have an effect (albeit small) on the apparent axial position. Second, the LAFPA design necessitates a thick-lipped nozzle, which may serve as a reflecting surface, making upstream traveling waves appear to be originating from the nozzle region. Most important, one needs to be cognizant of

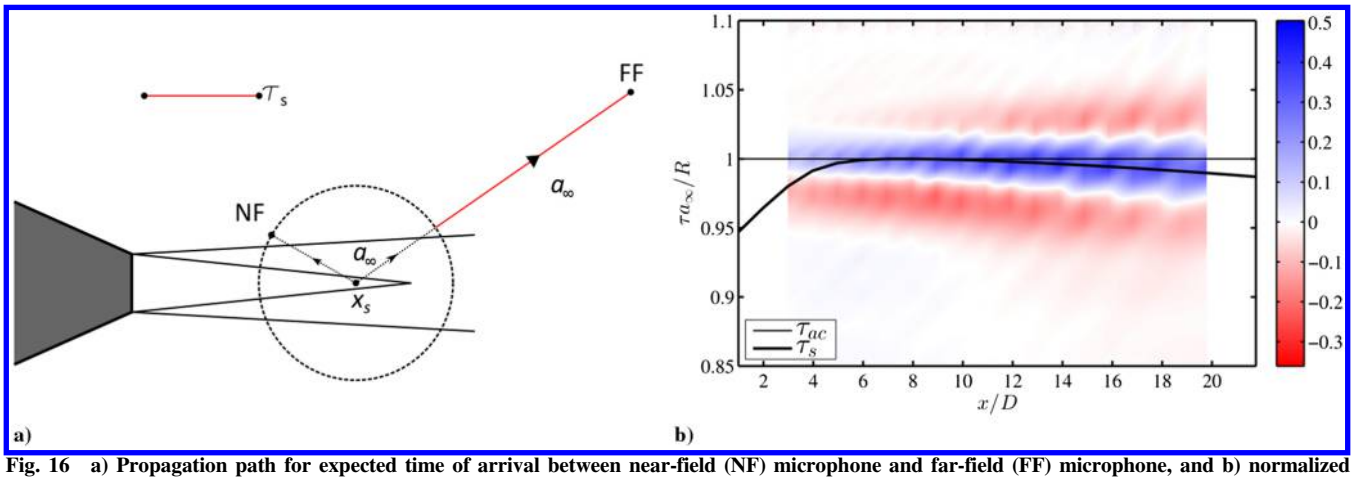

Fig. 16 a) Propagation path for expected time of arrival between near-field (NF) microphone and far-field (FF) microphone, and b) normalized correlations in the unforced jet to the far field at 30 deg.

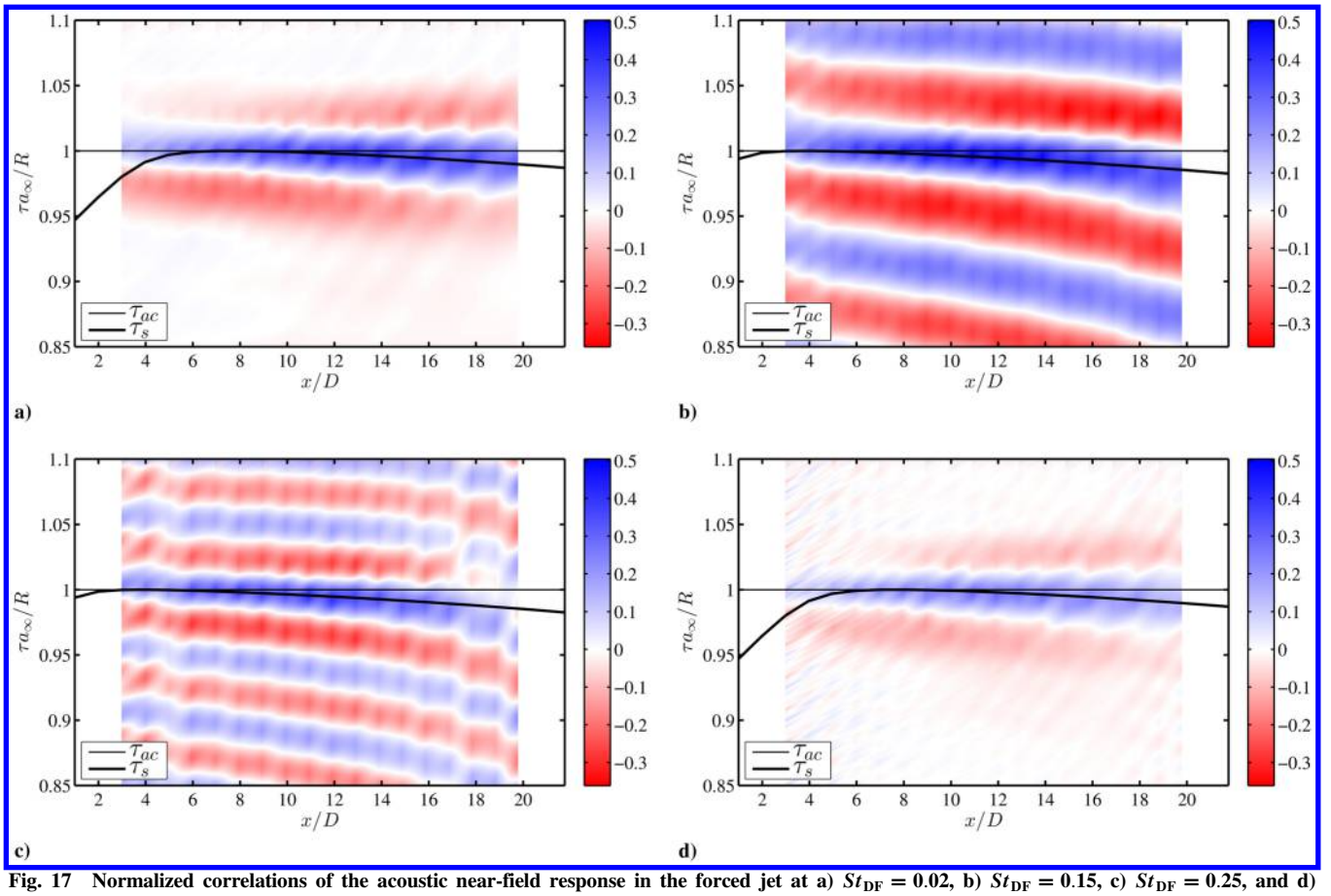

Fig. 17 Normalized correlations of the acoustic near-field response in the forced jet at a) $St_{DF} = 0.02$, b) $St_{DF} = 0.15$, c) $St_{DF} = 0.25$, and d) $St_{DF} = 0.50$; the assumed source location was set to $4D$, $1D$, $1D$, and $4D$, respectively.

the limits of a correlation analysis; these results indicate the dominant noise-source region in terms of time-averaged correlation to far-field aft angles, but this does not strictly mean that no noise emission occurs further downstream, or that this region is stationary over all time.

Similar calculations were carried out for the forced jets, and the results are shown in Fig. 17. For very low St_{DF}, for which the structures evolve independently before passing through the end of the potential core (Fig. 17a), the correlation regions are nearly unchanged from the unforced jet. As before, the upstream peak correlations match with τ_{ac}, whereas the downstream match with τ_s with x_s set to $4D$, again indicating that the acoustic fluctuations measured in the downstream are predominantly being generated upstream, before the end of the potential core. As the excitation frequency is increased and the generated structures begin undergoing significant linear interactions as they advect through the mixing layer upstream of the end of the potential core (Figs. 17b and 17c), the assumed source region x_s must be shifted upstream to $1D$ for τ_s to continue to match with the peak correlation values in the downstream. This upstream shift is unsurprising, given that it has already been shown that the higher-frequency structures saturate and begin to decay further upstream than the lower-frequency structures (see Fig. 12). By $St_{DF} = 0.50$, however, the correlation regions have returned to their unforced state — reinforcing the previous hypothesis that the structures generated by this forcing no longer constitute the dominant source in this jet.

C. Intermittency of the Response

Up to this point, our analysis has relied on some sort of temporal averaging: either the phase averaging, the sliding convolution inherent in two-point correlations, or even the time integral necessary for the computation of the PSD. This greatly reduces the complexity of our analysis of the turbulent jet, although it comes at a significant cost in terms of the information lost. As other researchers have shown [9,44], subsonic jet noise is a highly intermittent phenomenon, the fine details of which may be smeared or completely masked by this temporal averaging.

Wavelet analysis, in which a user-defined mother wavelet is used as the basis function for the transform, has been used by numerous researchers to investigate the time-domain behavior of temporally localized phenomena. By using a basis, which is localized in both time and space, wavelet analysis overcomes many of the drawbacks of the Fourier-based spectrogram method (sliding Fourier transform). An excellent overview of wavelet data analysis may be found in Torrence and Compo [45], upon which the wavelet software used in this study was based. For this analysis, the modified Morlet wavelet was chosen as the mother wavelet, due to its good localization in both the time and frequency domains. The continuous-wavelet transform (computed in the Fourier domain) was performed on a continuous block of data corresponding to 50 excitation periods in the case of the forced jet. For the unforced jet, a 41 ms (8192 points) block of data was used. (This corresponds to roughly nine excitation periods at $St_{DF} = 0.02$, and 230 excitation periods at $St_{DF} = 0.50$.)

Sample results for the unforced jet can be found in Fig. 18, in which the wavelet power has been plotted as a function of nondimensionalized time and nondimensionalized pseudofrequency for the hydrodynamic and acoustic fields upstream ($x/D = 3$) and downstream ($x/D = 8$) of the end of the potential core. Both the hydrodynamic and acoustic fields are observed to be composed of temporally localized bursts of energy. This description of turbulence is not new, and it has been shown that the frequency- and temporally localized basis functions used in the wavelet transform are superior at identifying coherent structures and compressing the information in the turbulent field as compared to the Fourier basis [46]. The dominant energy of the hydrodynamic field upstream of the end of the potential core is broadband, existing primarily over a range of scales

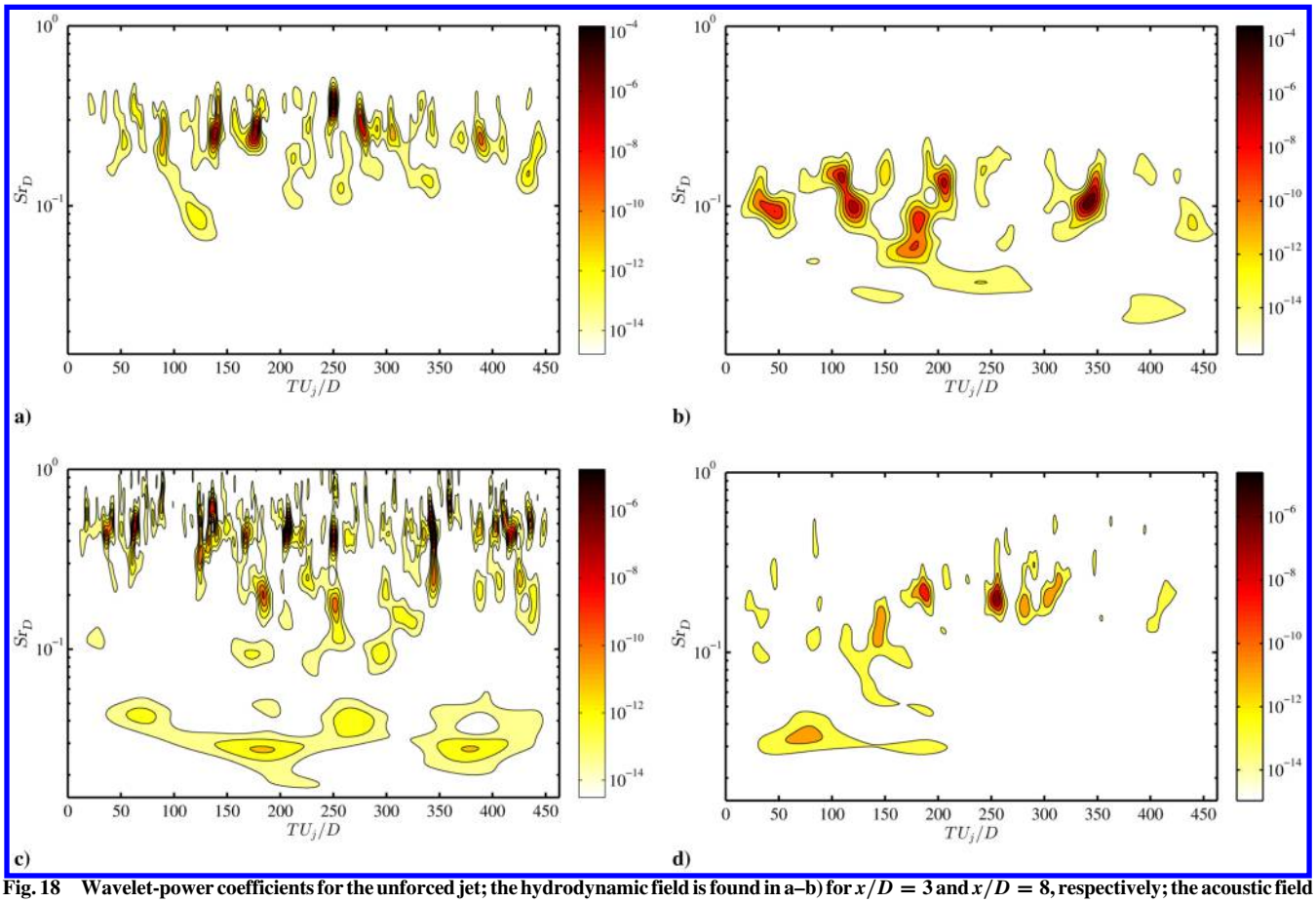

Fig. 18 Wavelet-power coefficients for the unforced jet; the hydrodynamic field is found in a–b) for $x/D = 3$ and $x/D = 8$, respectively; the acoustic field is found in c–d), again for the same respective locations.

of roughly $0.1 < St < 0.4$. A shift to lower frequencies of the dominant-energy-containing scales is observed with increasing axial distance; this is in agreement with the evolution of the Fourier PSD [10]. It should also be noted that the frequency of occurrence of the high-energy bursts is also diminished with axial distance — the coherent structures are becoming more intermittent. The interpretation of the evolution of the acoustic field with axial distance is not so straightforward, owing to the spherical propagation of the acoustic waves. Nonetheless, a similar shift away from high-frequency content energy bursts with downstream distance is apparent in the acoustic field.

The results for the impulse-forced jet ($St_{\mathrm{DF}} = 0.02$) can be found in Fig. 19 for the same axial locations. In the case of the hydrodynamic field upstream of the end of the potential core, regularly spaced striations are observed in the wavelet-power spectrum, corresponding to the coherent, independently evolving structures generated by the excitation (refer to Fig. 6). The structures themselves have a characteristic frequency much higher than the excitation frequency, roughly $St_{\mathrm{DF}} = 0.15$, which corresponds to the characteristic period of the phase-averaged waveform observed in Fig. 6a for this excitation frequency. In fact, the characteristic frequencies of the structures generated by the impulse excitation are quite similar to the structures in the unforced jet at this location (Fig. 18a), indicating that the structures generated by excitation are evolving in the same manner as the structures in the natural jet. There is a noticeable shift in the energy content of the structures to lower St_D downstream of the end of the potential core, although a semiregular pattern is still detectable (no longer at the excitation frequency).

The impulse forcing has a little effect on the overall composition or organization of the energy content of the acoustic field. Given that the structures generated by the excitation are evolving just as the natural turbulence, a similarity of the dominant-energy-containing frequencies (or, in this case, the lack of a clear dominant-energy range) between the forced and unforced jets is expected. It should be noted, however, that the impulse forcing is not producing a clear temporal regularization of the energy content in the acoustic field, as it has in the hydrodynamic. This result may seem to contradict those shown previously, in which the phase averaging of the acoustic field showed a coherent response to the impulse forcing. It is improbable that the phase-averaged acoustic response to periodic forcing could be constructed as a superposition of impulse responses if the impulse response itself did not actually correspond to anything physical. Likely, this phase-averaged response to impulse forcing represents the average response of the large-scale structure generated by the forcing to the interactions with structures over the entire range of (noise producing) scales present in the turbulent jet. The instantaneous turbulent field still very much affects the noise-generation process, and hence, the structures seeded by the excitation do not undergo identical evolutions. However, the sound-generation mechanism is unchanged, and, as a result, a semiconsistent acoustic waveform shape and source region can be recovered.

In the case of the periodically forced jet where the structures are linearly interacting (Fig. 20), a regularization of the hydrodynamic field is again observed in the upstream position. In this case, however, a marked shift in energy content is found in the downstream position. Here, the dominant energy has no relationship to the forced structures, likely due to the decay and breakdown of the seeded structures. (Shifting the color axis can identify some structures generated by the excitation as still being present, but their energy is at least two orders of magnitude less than the peak energy at this location.) Unlike the impulse-forced jet, the acoustic field of the periodically forced jet exhibits consistent energy bands at the excitation frequency and, in some cases, its second harmonic. Although the events in the acoustic field are less consistent than those in the hydrodynamic, they still represent a semicoherent response to the excitation. The coherent interactions produced by the periodic

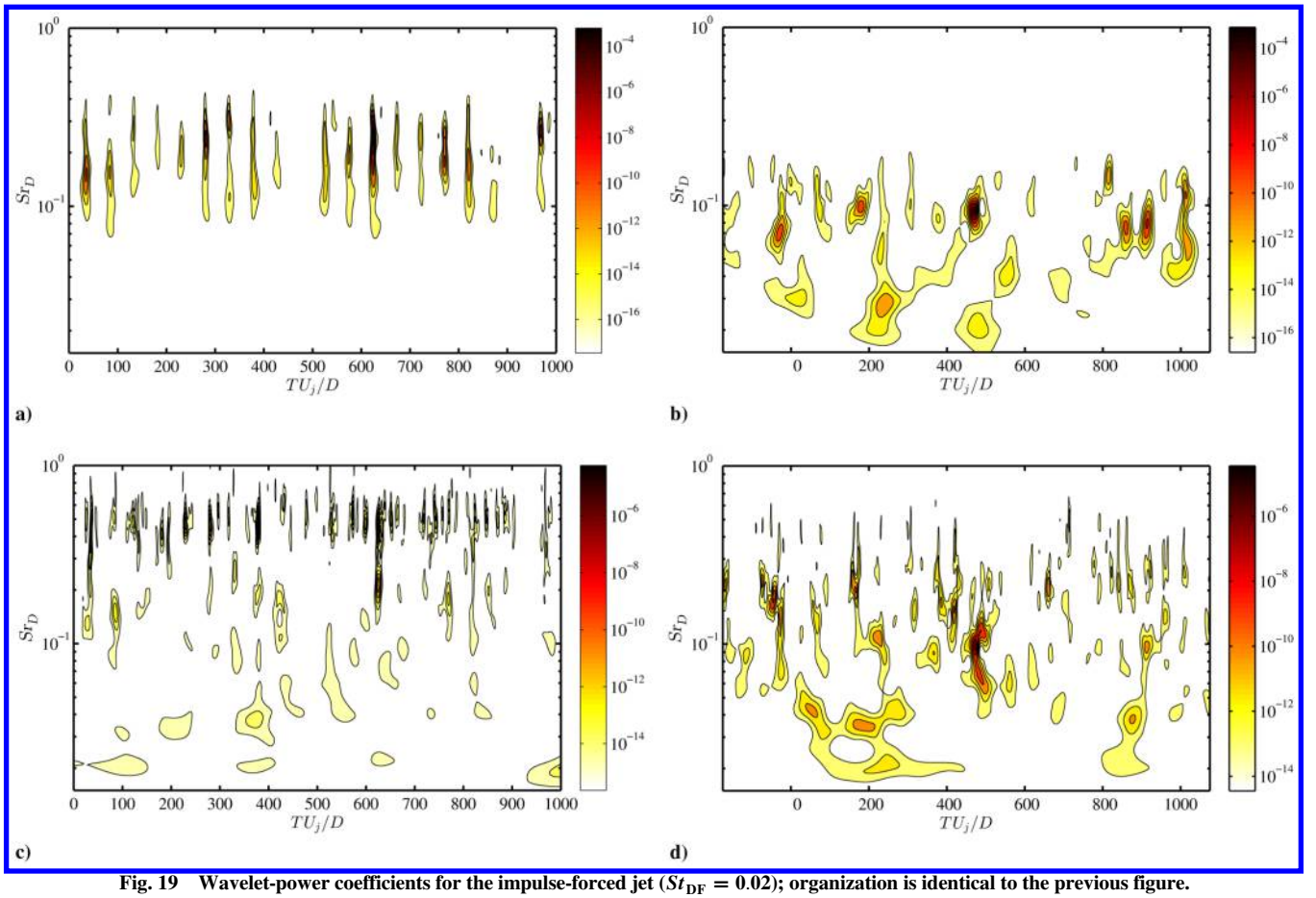

Fig. 19 Wavelet-power coefficients for the impulse-forced jet ($St_{DF} = 0.02$); organization is identical to the previous figure.

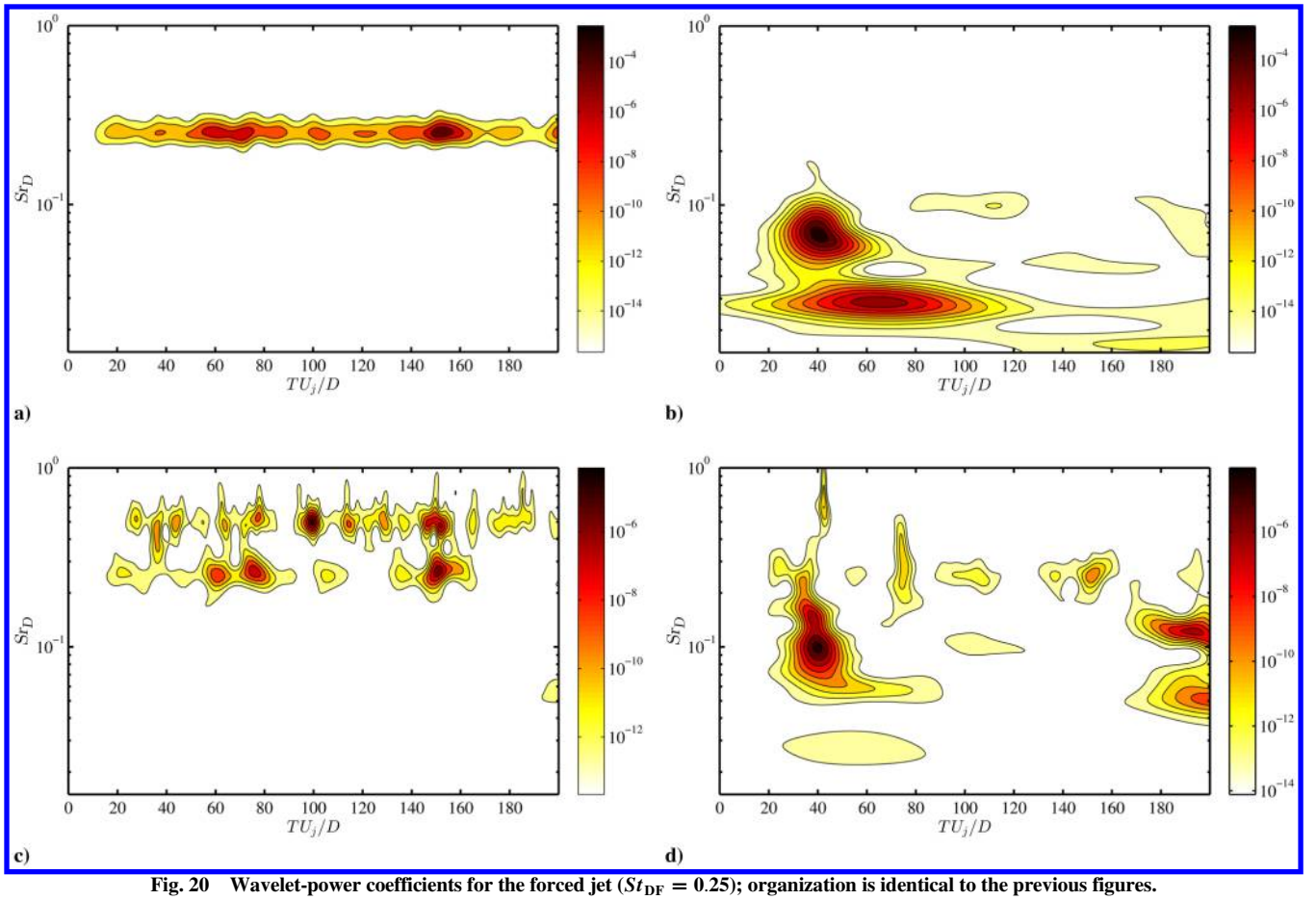

Fig. 20 Wavelet-power coefficients for the forced jet ($St_{DF} = 0.25$); organization is identical to the previous figures.

forcing are themselves producing, either directly or indirectly, relatively coherent acoustic radiation. This is in contrast to the incoherent interactions in the impulse-forced jet, which are producing incoherence radiation. Of course, the structures generated by the impulse-forcing are interacting with the incoherent background turbulence.

IV. Conclusions

The LAFPAs used in this study provide a unique tool to investigate the dynamics of large-scale structures, the noise sources, and the radiated noise; the well-defined actuation phase enables phase averaging of the pressure signal. Hence, time-resolved (more precisely, phase-resolved) measurements over an entire region of the near field may be acquired and correlated using minimal sensors, providing additional insight into the noise sources than the conventional two-point correlations.

Previous studies [26] had found that forcing at very low frequencies (impulse forcing), the structures evolve independently as they advect through the shear layer, representing the impulse response of the jet to a perturbation. As the excitation frequency is raised, the generated structures begin to interact before passing through the end of the potential core. The waveform amplitude and shape in this excitation regime ($0.15 \leq St_{DF} \leq 0.50$) could be well predicted by a linear superposition of the impulse response of the jet, indicating that the structure dynamics were predominantly linear in nature. The current results showed that the excitation produces coherent, large-scale structures that grow, interact, decay, and generate radiation to the far field. Two-point correlations between the near field and the far field at aft angles showed correlation regions matching the characteristics of convecting large-scale structures in the upstream measurement domain and acoustic radiation in the downstream. Aside from a slight upstream shift in the apparent source region, the correlations showed little characteristic changes over the range of Strouhal numbers explored in this study, suggesting a consistent dominant-source mechanism for the noise-generation process between the independently evolving and linearly interacting structures.

By applying a wave-number/frequency filter to the near-field measurements along each microphone-array position, the near-field pressure can be decomposed into its constitutive hydrodynamic and acoustic components based on the phase velocity. An examination of the spectra for the individual components revealed crossover between the spectral amplitudes at the critical frequency identified by previous researchers, as well as changes in the acoustic spectra in relation to the end of the potential core that match the previously observed features of the far-field spectra. Subsequent phase averaging of the decomposed acoustic near field, as well as two-point correlations with the far field, indicated that the excitation resulted in acoustic waves, which had their origins in the upstream portion of the jet, just before the end of the potential core. However, this should not be interpreted as meaning that this is the only region in which noise generation occurs, rather that the noise generated in this region correlates best with the far-field acoustic at aft angles. The apparent dominant-source region was observed to shift upstream with higher frequencies, in agreement with past results. As with the structures themselves, the acoustic response to periodic forcing could be well modeled as a linear superposition of the fundamental response; this strongly suggests a consistent source mechanism over the range of large-scale structures encountered in this study.

An investigation of the temporal intermittency of the response of a jet by way of wavelet analysis found that the excitation, either impulse or periodic, produced a strong regularization of the energy in the hydrodynamic field. The persistence of these highly energetic events (which correspond to the coherent large-scale structures generated by the excitation) was observed to decrease in axial distance with increasing excitation frequency. Excitation in the impulse regime, in which the generated structures do not interact coherently nor exhibit a consistent disintegration as they pass through the end of the potential core, produces little change in the energy composition of the acoustic field over the baseline jet. In this case, highly intermittent acoustic events, over a broad range of scales, are observed. Increasing the excitation frequency, such that the structures began linearly and coherently interacting, resulted in a regularization of the acoustic field.

Acknowledgment

The support of this work by the U.S. Air Force Office of Scientific Research (Rengasamy Ponnappan and John Schmisseur) is much appreciated.

References

[1] Lighthill, M. J., "On Sound Generated Aerodynamically. I. General Theory," *Proceedings of the Royal Society of London, Series A: Mathematical and Physical Sciences*, Vol. 211, No. 1107, 1952, pp. 564–587. doi:10.1098/rspa.1952.0060

[2] Tam, C. K. W., Viswanathan, K., Ahuja, K., and Panda, J., "The Source of Jet Noise: Experimental Evidence," *Journal of Fluid Mechanics*, Vol. 615, Nov. 2008, pp. 253–292. doi:10.1017/S0022112008003704

[3] Mollo-Christensen, E., "Jet Noise and Shear Flow Instability Seen from an Experimenter's Viewpoint," *Journal of Applied Mechanics*, Vol. 34, No. 1, 1967, pp. 1–7. doi:10.1115/1.3607624

[4] Crow, S. C., and Champagne, F. H., "Orderly Structure in Jet Turbulences," *Journal of Fluid Mechanics*, Vol. 48, No. 3, 1971, pp. 547–591. doi:10.1017/S0022112071001745

[5] Brown, G. L., and Roshko, A., "On Density Effects and Large Structure in Turbulent Mixing Layers," *Journal of Fluid Mechanics*, Vol. 64, No. 4, 1974, pp. 775–816. doi:10.1017/S002211207400190X

[6] Jordan, P., and Colonius, T., "Wave Packets and Turbulent Jet Noise," *Annual Review of Fluid Mechanics*, Vol. 45, No. 1, 2013, pp. 173–195. doi:10.1146/annurev-fluid-011212-140756

[7] Crighton, D. G., and Huerre, P., "Shear-Layer Pressure Fluctuations and Superdirective Acoustic Sources," *Journal of Fluid Mechanics*, Vol. 220, No. 1, 1990, pp. 355–368. doi:10.1017/S0022112090003299

[8] Sandham, N. D., Morfey, C. L., and Hu, Z. W., "Nonlinear Mechanisms of Sound Generation in a Perturbed Parallel Jet Flow," *Journal of Fluid Mechanics*, Vol. 565, Oct. 2006, pp. 1–23. doi:10.1017/S0022112006001315

[9] Cavalieri, A. V. G., Jordan, P., Gervais, Y., Wei, M., and Freund, J. B., "Intermittent Sound Generation and Its Control in a Free-Shear Flow," *Physics of Fluids*, Vol. 22, No. 11, 2010, Paper 115113. doi:10.1063/1.3517297

[10] Arndt, R. E. A., Long, D. F., and Glauser, M. N., "The Proper Orthogonal Decomposition of Pressure Fluctuations Surrounding a Turbulent Jet," *Journal of Fluid Mechanics*, Vol. 340, June 1997, pp. 1–33. doi:10.1017/S0022112097005089

[11] Coiffet, F., Jordan, P., Delville, J., Gervais, Y., and Ricaud, F., "Coherent Structures in Subsonic Jets: A Quasi-Irrotational Source Mechanism?" *International Journal of Aeroacoustics*, Vol. 5, No. 1, 2006, pp. 67–89. doi:10.1260/147547206775220407

[12] Tinney, C. E., and Jordan, P., "The Near Pressure Field of Co-Axial Subsonic Jets," *Journal of Fluid Mechanics*, Vol. 611, Sept. 2008, pp. 175–204. doi:10.1017/S0022112008001833

[13] Grizzi, S., and Camussi, R., "Experimental Investigation of Pressure Fluctuations in the Near Field of Subsonic Jets at Different Mach and Reynolds Numbers," *18th AIAA/CEAS Aeroacoustics Conference*, AIAA Paper 2012-2257, 2012.

[14] Kuo, C.-W., Buisson, Q., McLaughlin, D. K., and Morris, P. J., "Experimental Investigation of Near-Field Pressure Fluctuations Generated by Supersonic Jets," *19th AIAA/CEAS Aeroacoustics Conference*, AIAA Paper 2013-2033, May 2013.

[15] Samimy, M., Adamovich, I., Webb, B., Kastner, J., Hileman, J., Keshav, S., and Palm, P., "Development and Characterization of Plasma Actuators for High-Speed Jet Control," *Experiments in Fluids*, Vol. 37, No. 4, 2004, pp. 577–588. doi:10.1007/s00348-004-0854-7

[16] Utkin, Y. G., Keshav, S., Kim, J.-H., Kastner, J., Adamovich, I. V., and Samimy, M., "Development and Use of Localized Arc Filament Plasma Actuators for High-Speed Flow Control," *Journal of Physics D: Applied*

Physics, Vol. 40, No. 3, 2007, pp. 685–694.
doi:10.1088/0022-3727/40/3/S06

[17] Samimy, M., Kim, J. H., Kastner, J., Adamovich, I., and Utkin, Y., "Active Control of a Mach 0.9 Jet for Noise Mitigation Using Plasma Actuators," *AIAA Journal*, Vol. 45, No. 4, 2007, pp. 890–901.
doi:10.2514/1.27499

[18] Kim, J. H., Kastner, J., and Samimy, M., "Active Control of a High Reynolds Number Mach 0.9 Axisymmetric Jet," *AIAA Journal*, Vol. 47, No. 1, 2009, pp. 116–128.
doi:10.2514/1.36801

[19] Samimy, M., Kim, J. H., Kastner, J., Adamovich, I., and Utkin, Y., "Active Control of High-Speed and High-Reynolds-Number Jets Using Plasma Actuators," *Journal of Fluid Mechanics*, Vol. 578, No. 1, 2007, pp. 305–330.
doi:10.1017/S0022112007004867

[20] Kim, J.-H., and Samimy, M., "Effects of Active Control on the Flow Structure in a High Reynolds Number Supersonic Jet," *International Journal of Flow Control*, Vol. 1, No. 2, 2009, pp. 99–117.
doi:10.1260/175682509788913344

[21] Samimy, M., Kim, J.-H., Kearney-Fischer, M., and Sinha, A., "Acoustic and Flow Fields of an Excited High Reynolds Number Axisymmetric Supersonic Jet," *Journal of Fluid Mechanics*, Vol. 656, Aug. 2010, pp. 507–529.
doi:10.1017/S0022112010001357

[22] Kim, J.-H., Kearney-Fischer, M., Samimy, M., and Gogineni, S., "Far-Field Noise Control in Supersonic Jets Using Conical and Contoured Nozzles," *Journal of Engineering for Gas Turbines and Power*, Vol. 133, No. 8, 2011, Paper 081201.
doi:10.1115/1.4002811

[23] Kearney-Fischer, M., Kim, J.-H., and Samimy, M., "Noise Control of a High Reynolds Number High Speed Heated Jet Using Plasma Actuators," *International Journal of Aeroacoustics*, Vol. 10, Nos. 5, 6, 2011, pp. 635–658.
doi:10.1260/1475-472X.10.5-6.635

[24] Samimy, M., Kearney-Fischer, M., Kim, J.-H., and Sinha, A., "High-Speed and High-Reynolds-Number Jet Control Using Localized Arc Filament Plasma Actuators," *Journal of Propulsion and Power*, Vol. 28, No. 2, 2012, pp. 269–280.
doi:10.2514/1.B34272

[25] Kearney-Fischer, M., Kim, J.-H., and Samimy, M., "A Study of Mach Wave Radiation Using Active Control," *Journal of Fluid Mechanics*, Vol. 681, Aug. 2011, pp. 261–292.
doi:10.1017/jfm.2011.196

[26] Sinha, A., Alkandry, H., Kearney-Fischer, M., Samimy, M., and Colonius, T., "The Impulse Response of a High-Speed Jet Forced with Localized Arc Filament Plasma Actuators," *Physics of Fluids*, Vol. 24, No. 12, 2012, Paper 125104.
doi:10.1063/1.4772191

[27] Hahn, C., "Design and Validation of the New Jet Facility and Anechoic Chamber," M.S. Thesis, Dept. of Mechanical Engineering, The Ohio State Univ., Columbus, OH, 2011.

[28] Kearney-Fischer, M., Kim, J.-H., and Samimy, M., "Control of a High Reynolds Number Mach 0.9 Heated Jet Using Plasma Actuators," *Physics of Fluids*, Vol. 21, No. 9, 2009, Paper 095101.
doi:10.1063/1.3210771

[29] Hahn, C., Kearney-Fischer, M., and Samimy, M., "On Factors Influencing Arc Filament Plasma Actuator Performance in Control of High Speed Jets," *Experiments in Fluids*, Vol. 51, No. 6, 2011, pp. 1591–1603.
doi:10.1007/s00348-011-1172-5

[30] Guitton, A., Kerherve, F., Jordan, P., and Delville, J., "The Sound Production Mechanism Associated with Coherent Structures in Subsonic Jets," *AIAA/CEAS 14th Aeroacoustics Conference*, AIAA Paper 2008-2892, May 2008.

[31] Alkandry, H., Crawley, M., Sinha, A., Kearney-Fischer, M., and Samimy, M., "An Investigation of the Irrotational Near Field of an Excited High-Speed Jet," *51st AIAA Aerospace Sciences Meeting*, AIAA Paper 2013-0325, Jan. 2013.

[32] Freund, J. B., "Noise Sources in a Low-Reynolds-Number Turbulent Jet at Mach 0.9," *Journal of Fluid Mechanics*, Vol. 438, July 2001, pp. 277–305.
doi:10.1017/S0022112001004414

[33] Crawley, M., and Samimy, M., "Decomposition of the Near-Field Pressure in an Excited Subsonic Jet," *20th AIAA/CEAS Aeroacoustics Conference*, AIAA Paper 2014-2342, June 2014.

[34] Hussain, A. K. M. F., and Reynolds, W. C., "The Mechanics of an Organized Wave in Turbulent Shear Flow," *Journal of Fluid Mechanics*, Vol. 41, No. 2, 1970, pp. 241–258.
doi:10.1017/S0022112070000605

[35] Veltin, J., Day, B. J., and McLaughlin, D. K., "Correlation of Flowfield and Acoustic Field Measurements in High-Speed Jets," *AIAA Journal*, Vol. 49, No. 1, 2011, pp. 150–163.
doi:10.2514/1.J050583

[36] Kambe, T., and Minota, T., "Acoustic Wave Radiated by Head-On Collision of Two Vortex Rings," *Proceedings of the Royal Society of London, Series A: Mathematical and Physical Sciences*, Vol. 386, No. 1791, 1983, pp. 277–308.

[37] Bogey, C., and Bailly, C., "An Analysis of the Correlations Between the Turbulent Flow and the Sound Pressure Fields of Subsonic Jets," *Journal of Fluid Mechanics*, Vol. 583, July 2007, pp. 71–97.
doi:10.1017/S002211200700612X

[38] Hall, J. W., Pinier, J., Hall, A. E., and Glauser, M., "Two-Point Correlations of the Near and Far-Field Pressure in a Transonic Jet," *ASME 2006 Joint U.S.–European Fluids Engineering Summer Meeting*, FEDSM 2006-98458, July 2006.

[39] Kœnig, M., Cavalieri, A. V. G., Jordan, P., and Gervais, Y., "Intermittency of the Azimuthal Components of the Sound Radiated by Subsonic Jets," *AIAA/CEAS 17th Aeroacoustics Conference*, AIAA Paper 2011-2746, June 2011.

[40] Juve, D., Sunyach, M., and Comte-Bellot, G., "Filtered Azimuthal Correlations in the Acoustic Far Field of a Subsonic Jet," *AIAA Journal*, Vol. 17, No. 1, 1979, pp. 112–113.
doi:10.2514/3.61076

[41] Suzuki, T., and Colonius, T., "Instability Waves in a Subsonic Round Jet Detected Using a Near-Field Phased Microphone Array," *Journal of Fluid Mechanics*, Vol. 565, Oct. 2006, pp. 197–226.
doi:10.1017/S0022112006001613

[42] Ukeiley, L. S., and Ponton, M. K., "On the Near Field Pressure of a Transonic Axisymmetric Jet," *International Journal of Aeroacoustics*, Vol. 3, No. 1, 2004, pp. 43–65.
doi:10.1260/147547204323022257

[43] Hileman, J. I., Thurow, B. S., Caraballo, E. J., and Samimy, M., "Large-Scale Structure Evolution and Sound Emission in High-Speed Jets: Real-Time Visualization with Simultaneous Acoustic Measurements," *Journal of Fluid Mechanics*, Vol. 544, No. 1, 2005, pp. 277–307.
doi:10.1017/S002211200500666X

[44] Kearney-Fischer, M., Sinha, A., and Samimy, M., "Intermittent Nature of Subsonic Jet Noise," *AIAA Journal*, Vol. 51, No. 5, 2013, pp. 1142–1155.
doi:10.2514/1.J051930

[45] Torrence, C., and Compo, G. P., "A Practical Guide to Wavelet Analysis," *Bulletin of the American Meteorological Society*, Vol. 79, No. 1, 1998, pp. 61–78.
doi:10.1175/1520-0477(1998)079<0061:APGTWA>2.0.CO;2

[46] Farge, M., "Wavelet Transforms and Their Applications to Turbulence," *Annual Review of Fluid Mechanics*, Vol. 24, No. 1, 1992, pp. 395–458.
doi:10.1146/annurev.fl.24.010192.002143

M. Glauser
Associate Editor